Evaluating the paleoenvironmental significance of sediment grain size in Bering Sea sediments

during Marine Isotope Stage 11

- 4 Natalie S. Thompson<sup>a</sup> and Beth E. Caissie<sup>a,b,\*</sup>
- 5 <sup>a</sup> Department of Geological and Atmospheric Sciences, Iowa State University, Ames, IA, USA
- 6 b present address: U.S. Geological Survey, Menlo Park, CA
  - \*Corresponding author: Beth E. Caissie, bcaissie@usgs.gov

## **ABSTRACT**

Grain size is an important textural property of sediments and is widely used in paleoenvironmental studies as a means to infer changes in the sedimentary environment. However, grain size parameters are not always easy to interpret without a full understanding of the factors that influence grain size. Here, we measure grain size in sediment cores from the Bering slope and the Umnak Plateau, and review the effectiveness of different grain size parameters as proxies for sediment transport, current strength, and primary productivity, during a past warm interval (Marine Isotope Stage 11, 424-374 ka).

In general, sediments in the Bering Sea are hemipelagic, making them ideal deposits for paleoenvironmental reconstructions, but there is strong evidence in the grain size distribution for contourite deposits between  $\sim$ 408-400 ka at the slope sites, suggesting a change in bottom current transport at this time. We show that the grain size of coarse (>150  $\mu$ m) terrigenous sediment can be used effectively as a proxy for ice rafting, although it is not possible to distinguish between iceberg and sea ice rafting processes, based on grain size alone. We find that the mean grain size of bulk sediments can be used to infer changes in productivity on glacial-interglacial timescales, but the size and preservation of diatom valves also exert a control on mean grain size. Lastly, we show that the mean size of sortable silt (10-63  $\mu$ m) is not a valid proxy for bottom current strength in the Bering Sea, because the input of icerafted silt confounds the sortable silt signal.

**KEYWORDS:** Marine Isotope Stage 11; Bering Sea; Marine sediments; Grain size; Ice-rafted debris;

Contourites

29

30

31

32

33

34

35

36

37

38

39

40

41

42

43

44

45

46

47

48

49

50

51

52

27

28

## INTRODUCTION

Marine sediments provide valuable records of Earth's climate history over long (millions of years) time scales and are thus a highly valuable tool in paleoceanographic and paleoclimatic reconstructions. In particular, the textural properties of marine sediments can help us to gain a deeper understanding of the different sedimentary processes that operate under changing environmental conditions (Poppe et al. 2006; Rothwell and Rack 2006). Grain size is a fundamental property of ocean sediments that is widely used in paleoceanographic studies, most notably as a proxy for sediment source, transport, and depositional processes. For example, variations in the grain size of marine sediments have been related to changes in productivity (Aiello and Ravelo 2012; Muhong et al. 2005; Warner and Domack 2002), fluvial discharge (Briceño-Zuluaga et al. 2016; Carlin et al. 2019; Weltje and Prins 2003), aeolian dust input (Briceño-Zuluaga et al. 2016; Holz et al. 2007; Serno et al. 2014; Stuut et al. 2014; Weltje and Prins 2003), the strength and flow speed of tidal and bottom currents (e.g., McCave et al. 1995, 2017; Hoffman et al. 2019; Tegez et al. 2014; Voigt et al. 2016; Kawaguchi et al. 2020), and bioturbation, which can result in sediment sorting (Carter et al. 2009). Sediment grain size may also be controlled by internal slope processes such as gravity or earthquake induced down-slope transport and turbidity (Goldfinger et al. 2017; Sequeiros et al. 2018). In addition, grain size is key to interpreting sediment composition (Aiello and Ravelo 2012; Sval'nov and Alekseeva 2006), and can be used to help distinguish between different types of deep-water sediment facies (e.g., Stow and Smillie 2020; Stow and Tabrez 1998). Of particular importance in high latitude settings is the information that grain size can provide about glacial and sea ice extent. Numerous studies have used sediment grain size records to infer the ice rafting history of a region (e.g., Andrews and Principato 2002; deGelleke et al. 2013; Kim et al. 2018;

Nürnberg et al. 1994; O'Regan et al. 2014; Sakamoto et al. 2005; St. John et al. 2008). By way of

example, St. John et al. (2008) used grain size to reconstruct the Cenozoic history of ice rafting in the Arctic Ocean and showed that ice was present in the Arctic Ocean as early as the middle Eocene, whilst Sakamoto et al. (2005) used the grain size distribution of terrigenous particles to reconstruct sea ice expansion events in the Sea of Okhotsk over the past 100 ka.

Although grain size has the potential to be an extremely useful proxy, it is not always easy to interpret because of the multiple factors that influence grain size. Bering Sea sediments are a mix of biogenic, terrigenous, and volcanogenic sediments that likely reflect a wide range of transport and depositional processes, including vertical settling, winds, sea ice, icebergs, gravity flows, bottom currents, and other transport mechanisms (Takahashi et al. 2011). Here we show that Bering Sea grain size records can successfully be used to infer the sedimentary history of the Bering Sea during a past warm interval (Marine Isotope Stage 11; 424-374 ka). Marine Isotope Stage (MIS) 11 is the most recent interglacial period with orbital parameters similar to the Holocene, and is considered a partial analogue for current and future warming (Droxler and Farrell 2000; Berger and Loutre 2002; Loutre and Berger 2003; Masson-Delmotte et al. 2006; Bowen 2010), although it is important to recognize that the natural course of Holocene warming has been disrupted by anthropogenic activity (Ruddiman 2007; Palumbo et al. 2019; Cronin et al. 2019). We measure grain size in sediments from three core sites on the Bering slope and Umnak Plateau, which were obtained during Integrated Ocean Drilling Program (IODP) Expedition 323 in 2009. We calculate several grain size parameters for the sediments and review the limitations and effectiveness of these parameters to serve as a proxy for sediment facies, transport mechanisms such as ice rafting, bottom current strength, and paleoproductivity.

73

74

75

76

77

78

53

54

55

56

57

58

59

60

61

62

63

64

65

66

67

68

69

70

71

72

#### **REGIONAL SETTING**

## Location and oceanographic setting

The Bering Sea, located between Russia and Alaska, is a marginal sea of the North Pacific Ocean. It comprises a broad (>500 km), shallow continental shelf in the east, a narrow (<100 km) shelf to the west, a steep continental slope, and a deep abyssal basin, dissected by several large submarine rises (text-

fig. 1; Ben-Avraham and Cooper 1981; Stabeno et al. 1999). The Aleutian Island Arc forms a boundary between the Bering Sea and the North Pacific, but water mass exchange occurs through passes in the Aleutian Islands, linking Bering Sea conditions to those of the Pacific (Stabeno et al. 1999; Stabeno et al. 2016; Prants et al. 2019). To the north, the shallow (-50 m) Bering Strait serves as the only connection between the Pacific and Arctic Oceans (text-fig. 1).

79

80

81

82

83

84

85

86

87

88

89

90

91

92

93

94

95

96

97

98

99

100

101

102

103

104

General circulation in the Bering Sea basin is cyclonic, with much of the Pacific inflow balanced by outflow through Kamchatka Strait (text-fig. 1; Stabeno et al. 1999; Kinney and Maslowski 2012), although a substantial amount of surface water (~0.8 Sv) is also transported northward through the Bering Strait (Roach et al. 1995). Surface water masses in the Bering Sea are largely derived from inflow of the Alaska Coastal Current (ACC) and the Alaskan Stream through several relatively shallow passes along the Aleutian Arc (Stabeno et al. 1999; Ladd et al. 2005; Stabeno et al. 2009; Kinney and Maslowski 2012). Originating in the Gulf of Alaska, the ACC is a relatively warm, fresh, and nutrient-poor current that enters the Bering Sea primarily through the shallow Unimak Pass in the eastern Aleutians and flows northward across the Bering shelf between 50 and 100 m depth (Stabeno et al. 2016). The Alaskan Stream is a deeper (up to 5,000 m), stronger current that flows into the Bering Sea primarily through Amchitka and Amukta Passes, which are deeper and farther west than Unimak Pass. Tidal mixing in these passes brings nutrients as well as heat to the Bering Sea from the Pacific. Mesoscale eddies also carry nutrients northward and drive primary productivity in the southeastern Bering Sea and along the slope (Prants et al. 2019; Stabeno et al. 2005). North of the Aleutian Islands, the Alaskan Stream forms the Aleutian North Slope Current (ANSC) (Prants et al. 2019). In turn, the northeastward flow of the ANSC is diverted northwestward as it nears the shallow continental shelf at Umnak Plateau and forms the Bering Slope Current (BSC), the eastern boundary current of the Bering Sea gyre (text-fig. 1; Stabeno et al. 1999, 2009; Kinney and Maslowski 2012; Mauch et al. 2018). The BSC is a deep current, observed flowing at velocities up to 0.033 m/s at 1,000 m depth (Johnson et al. 2004). As it flows along the continental slope, a portion of the BSC is upwelled by Ekman transport to supply critical nutrients from depth to the shelf (Danielson et al. 2012), often via canyons such as Navarin and Zhemchug (text-fig. 1; Stabeno et al.

2016). The resulting nutrient-rich waters contribute to the high rates of biological productivity in the Bering Sea, which is one of the most productive marine ecosystems in the world (Brown and Arrigo 2012, 2013; Loughlin et al. 1999; Sigler et al. 2010; Stabeno et al. 2019).

108

109

110

111

112

113

114

115

116

117

118

119

120

121

122

123

124

125

126

127

128

129

105

106

107

#### Sedimentation in the Bering Sea

Sediments in the Bering Sea are primarily a mix of biogenic and fine-grained siliciclastic particles, whilst secondary components of the sediment include volcanogenic material, sand-sized siliciclastics, and ice-rafted debris (IRD) (Aiello and Rayelo 2012; Takahashi et al. 2011). The biogenic materials largely comprise siliceous diatom frustules, with lesser contributions from other microfossils, including foraminifera, radiolarians, and sponge spicules (Aiello and Ravelo 2012; Takahashi et al. 2011). Terrigenous sediments in the Bering Sea are mostly derived from the surrounding landmasses; in particular, the Alaskan mainland, the Alaskan Peninsula, and eastern Siberia, and to a lesser extent, from the Aleutian Arc, which is the primary source of volcanogenic input to the region. These sediments are transported to the Bering shelf by aeolian and fluvial processes, as well as ice rafting. (Asahara et al. 2012; Nagashima et al. 2012; Naidu and Mowatt 1983; Wang et al. 2016). In the North Pacific today, wind-blown aerosols are largely restricted to the vicinity of their source environments, and aeolian input of desert dust from the Asian continent is minimal (0.5-1 g m<sup>2</sup> yr<sup>-1</sup>) (Mahowald et al. 2005; Serno et al. 2014), although there is evidence for enhanced dust fluxes during past glacial periods (Riethdorf et al. 2013; Shaffer and Lambert 2018). Major rivers, including the Yukon, Kuskokwim and Anadyr, discharge millions of tons of sediment — mostly clay, silt, and fine sand-sized siliciclastics — to the continental shelf; in particular, the Yukon River provides ~63% of the total sediment load to the Bering Sea (text-fig. 1; Riethdorf et al. 2013). In addition, icebergs and sea ice may entrain and transport a mix of coarse and fine terrigenous material far offshore (e.g., Darby et al. 2011; Darby and Zimmerman 2008; Lisitzin 2002; Mager et al. 2013; Nürnberg et al. 1994; St. John et al. 2015). Sediment dispersal across the shelf is further influenced by wave energy, storms, and ocean currents (Nelson 1982).

#### **Core sites**

131

132

133

134

135

136

137

138

139

140

141

142

143

144

145

146

147

148

149

150

151

152

153

Sediment cores used in this study were retrieved from the Bering slope and the Umnak Plateau during IODP Expedition 323 to the Bering Sea in 2009 (text-fig. 1; Takahashi et al. 2011). Site U1345 is the northernmost of the three core sites and is located on an interfluve ridge near the shelf-slope break, just south of Navarin Canyon, at a water depth of 1,008 m (text-fig. 1; Takahashi et al. 2011). Site U1343 is situated on a topographic high (-1,953 m), which is isolated from the Bering Shelf by the Zhemchug Canyon (text-fig. 1; Takahashi et al. 2011). These two sites are located relatively close to the modern limit of winter sea ice on the northern shelf (text-fig. 1) and are situated within the highly productive Bering Sea Green Belt (Springer 1996; Takahashi et al. 2011). Both are primarily influenced by the BSC and experience both on-shelf and off-shelf current flow, depending on seasonal changes in wind direction (Danielson et al. 2012; Stabeno et al. 2016). Site U1339 is located in the southeastern Bering Sea, on the northwest flank of Umnak Plateau, at a water depth of 1,870 m. Today, Site U1339 is influenced by the Alaskan Stream, and by the relatively warm Aleutian North Slope Current, which inhibits the formation of sea ice in the region (text-fig. 1). Although no previous studies have examined surface and deep currents in the Bering Sea during Marine Isotope Stage 11, we theorize that oceanographic conditions would have been similar to today. However, on glacial-interglacial timescales, dramatic differences in sea level, atmospheric circulation, and sea ice would likely have led to changes in oceanographic circulation. Sea level may have been as much as 140 m below present during MIS 12 (Dutton et al. 2015), leading to closure of Unimak Pass and Bering Strait and leaving much of the Bering Shelf subaerially exposed. In addition, there is evidence for

substantial sea ice cover at Site U1339 and other regions of the Bering Sea in the past (Caissie et al. 2010, 2016; Cook et al. 2005; Katsuki and Takahashi 2005; Méheust et al. 2018; Nesterovich 2019; Onodera et al. 2016; Pelto et al. 2018; Sancetta et al. 1985).

#### **METHODS**

## Geochronology

The age models that we use were published in previous studies (Asahi et al. 2016; Cook et al. 2016). These age models were initially derived from the shipboard age models, which were developed using bio-and magnetostratigraphy (Takahashi et al. 2011). Oxygen isotope measurements from benthic foraminifera (Asahi et al. 2016; Cook et al. 2016) were then used to align the records to the global benthic stack (LR04; Lisiecki and Raymo 2005), and dates for each sample were obtained using linear interpolation between tie points (text-fig. 2). The age model for Site U1345 was subsequently improved by adding an extra tie point based on magnetic susceptibility (Caissie et al. 2016). Average sedimentation rates at the sites range from 29-45 cm/kyr at U1345 (Caissie et al. 2016), 12-38 cm/kyr at U1343 (Asahi et al. 2016), and 27-44 cm/kyr at U1339 (Cook et al. 2016).

#### **Grain size measurements**

Sediment was sampled every  $\sim$ 5 cm throughout MIS 11 (<200-year resolution), and every  $\sim$ 10 cm outside of MIS 11, from the primary splices at core sites U1343 (n = 239) and U1339 (n = 296). At U1345 (n = 97), grain size was analyzed every 23 cm (670-year resolution), in line with previously published records (Caissie et al. 2016). The grain size of these samples was measured using a Malvern Mastersizer Laser 3000, equipped with a Hydro MV dispersion tank. This instrument uses the principle of laser diffraction to determine the volume distribution of particles in 101 size bins ranging from 0.01 to 3,500  $\mu$ m, a size range sufficient to measure all particles sampled (particles larger than 3500  $\mu$ m rarely occur, except as dropstones).

Freeze-dried bulk sediments were massed to approximately 0.025 g and treated with the deflocculant sodium hexametaphosphate prior to being analyzed. To obtain the grain size of just the terrigenous fraction, a second set of samples were sequentially treated with 30% H<sub>2</sub>O<sub>2</sub>, 10% HCl, and 1 M NaOH to remove the organic, carbonate, and siliceous biogenic material, respectively, before grain size was measured (Sakamoto et al. 2005). Each sample was analyzed in triplicate by the Mastersizer and the

results were averaged. Bulk grain size records for Site U1345 were published previously by Caissie et al. (2016); we used the same samples to measure the grain size of the terrigenous fraction only.

The raw dataset provided by the Malvern software includes the volume % of grains in 109 bin sizes, as well as the  $10^{th}$  (Dx10),  $50^{th}$  (Dx50) and  $90^{th}$  (Dx90) percentiles. For simplicity, we grouped sediments into four size classes: clay ( $<2~\mu m$ ); silt (2-63  $\mu m$ ); sand (63-2000  $\mu m$ ) and gravel ( $>2000~\mu m$ ), based on a modified Udden-Wentworth scale (Blott and Pye 2001). We also calculated the volume distribution of grains in the 10-63  $\mu m$  size fraction (proxy for sortable silt), and the  $>150~\mu m$  and  $>250~\mu m$  size fractions (proxies for ice-rafted debris).

188

189

190

191

192

193

194

195

196

197

198

199

200

201

202

203

204

205

180

181

182

183

184

185

186

187

#### Statistical analyses

Additional grain size parameters, including mean size, sorting and skewness, were calculated in GRADISTAT, a program that allows for rapid analysis of grain size statistics by a variety of methods (Blott and Pve 2001). Here, we use the geometric (modified) Folk and Ward (1957) graphical measure, which provides a robust basis for routine comparisons of compositionally variable sediments (Blott and Pye 2001). A further advantage of the Folk and Ward method is the opportunity to convert parameter values to descriptive terms for the sediment. With this method, mean grain size is computed by averaging particle sizes at the 16<sup>th</sup>, 50<sup>th</sup>, and 84<sup>th</sup> percentile values (Folk and Ward 1957). Sorting, or standard deviation, is a measure of the spread of particles around the average. We applied the inclusive standard deviation of Folk and Ward (1957), which includes the 5th and 95th percentiles, to define a spread of 1.65 standard deviations on either side of the mean. Skewness is a measure of the asymmetry of the grain size distribution (Folk and Ward 1957). In a normal (symmetrical or near-symmetrical) distribution, the mean, median, and mode all coincide. By convention, skewness is measured in phi  $(\phi)$  units, where a positive skew indicates a tail in the direction of the fine particles, with the mean and median shifted towards finer grain sizes, whilst a negative skew indicates a tail in the direction of the coarse particles (McManus et al. 1988; Blott and Pye 2001). However, logarithmic and geometric skewness parameters are inversely related, so to avoid confusion, we replace the terms 'positive' and 'negative', with 'fine-skewed',

indicating an excess of fine particles, and coarse-skewed, indicating a tail of coarse particles (Blott and Pye 2001; text-fig. 3). Kurtosis - the expression of sorting in the tails relative to the central distribution - is not widely used in grain size interpretations, except to measure the non-normality of a distribution (Blatt et al. 1982; McLaren 1981; McManus et al. 1988), so we chose not to examine this parameter.

Blott and Pye (2001) urge caution when using grain size statistics to analyze multimodal sediments, suggesting that descriptors provided by the GRADISTAT software (e.g., mode, median, distribution spread) may be more reliable. However, as the above statistics are routinely used in studies of multimodal marine sediments (e.g., Cronan 1972; Martins and Barboza 2005; McLaren 1981; Schlee 1973; Warrier et al. 2016), we chose to include these measures in our analyses.

## Smear slide analyses

Smear slide analyses were conducted on a subset of samples from the three sites (n = 55), in order to gain a better understanding of the relationship between grain size and sediment composition. Following the methods of Takahashi et al. (2011), the biogenic and mineral components in 10 random fields of view were identified, using a Nikon ECLIPSE Ni transmitted light microscope at magnifications of 100x and 400x. In addition, the diatom content in smear slides from sites U1345 and U1339 - the two sites that differ most from one another - was identified, and the relative percent abundance of diatoms visually estimated (Table S1).

## **RESULTS**

#### **Sediment composition**

Takahashi et al. (2011) used shipboard core descriptions and low-resolution smear slide analyses to show that sediments in the Bering Sea are primarily a mix of terrigenous and biogenic particles. Results from our higher resolution smear slide analyses support these findings; we identified three main sediment compositions: siliciclastic (>60% siliciclastic material); mixed (sub-equal proportions of terrigenous and biogenic material); and biogenic (>60% biogenic material). The terrigenous sediments mainly consist of

clay- to silt-sized siliciclastics. Volcanogenic material, mostly in the form of tephra shards, and coarse (>150  $\mu$ m) siliciclastic minerals and rock fragments typically make up a small (<10%) proportion of the sediment. Biogenic sediments largely comprise siliceous diatom frustules, although other microfossils, including sponge spicules, radiolarians, and foraminifera, are present in lower abundances.

At Site U1345, sediments are more siliciclastic, with diatom content ranging from as little as 2% to a maximum of 78% (average 25%). In contrast, sediments at Site U1339 are more biogenic in composition; diatom content varies from 10 to 92% (average 56%) (Table S1). Sediments at Site U1343 represent something of an intermediate composition between U1345 and U1339, with a more equal mix of terrigenous and biogenic sedimentation.

#### Grain size parameters

## Size fractions

Sediments in the Bering Sea contain a wide range of particle sizes, from fine clays to coarse sands and gravel. Because the proportion of grains in each size class varies between samples, grain size distribution plots show a range of modal compositions, including polymodal, trimodal, bimodal, and rarely, unimodal, although typically, there is always one dominant mode. At all three sites, the majority of particles fall within the silt-sized fraction. Sand is the second most abundant size fraction, followed by clay, then gravel (Table 1; text-fig. 4). The volume % of silt-sized grains is slightly higher for bulk sediments, averaging 84.2, 78.7, and 77.5% at sites U1345, U1343, and U1339, respectively, compared to 71.9, 73.9, and 74.8% for terrigenous sediments (Table 1). In bulk sediments, the proportion of silt-sized grains is highest at Site U1345, and lowest at U1339, but when biogenic material is dissolved, this trend is reversed (Table 1; text-fig. 4). In bulk sediment samples, the volume % clay is relatively low at all sites, particularly at Site U1345, and the % sand is lowest at U1345 and highest at U1339. After removing biogenics, the volume % of clay-sized grains increases at all sites, and is highest at U1339, and lowest at U1345. In contrast, the % of sand-sized particles is highest at U1345, and lowest at U1339 (Table 1; text-fig. 4).

#### Statistical measures

Mean grain size values fall mostly within the silt-sized fraction, except for intervals of coarsening centered around 403.5 ka at sites U1345 and U1343 (text-fig. 5). Overall, mean grain size is highest at the northernmost site (U1345) (Table 1). The mean grain size of bulk sediments is higher at Site U1339 than at U1343, but for terrigenous sediments, mean grain size is higher at U1343 (Table 1). In general, mean grain size at sites U1345 and U1343 is similar for both bulk and terrigenous sediments, but at Site U1339, bulk sediments are coarser than terrigenous sediments (Table 1; text-fig. 5).

Sediments range from poorly to very poorly sorted (text-fig. 5). Typically, bulk sediments are better sorted, and more symmetrical, than terrigenous, especially at Site U1345 (Table 1; text-fig. 5), perhaps because the biogenic particles included in bulk samples have a smaller range of sizes (typically silt to fine sand). At all three sites, terrigenous sediments can mostly be described as very poorly sorted (Table 1; text-fig. 5). Overall, terrigenous sediments have a more symmetrical distribution at sites U1345 (60%) and U1343 (75%), compared to U1339, where only 51% of the samples have a symmetrical or near-symmetrical distribution. Average skewness values (0.11) for Site U1339 indicate that terrigenous sediments at this site are more coarse-skewed (Table 1; text-fig. 5). As not all samples are symmetrical, there is some variation between measures of central tendency (mean, median, mode), although mean and median grain size display broadly similar trends (text-fig. 5).

## **DISCUSSION**

Downcore variations in grain size distribution can be used to infer changes in the sedimentary environment (e.g., Aiello and Ravelo 2012; McLaren 1981; Pelto et al. 2018; Stow and Smillie 2020; Vaughn and Caissie 2017; Wang et al. 2015; Warrier et al. 2016). In this section, we test whether grain size is effective as a proxy for siliciclastic input, sediment transport, ice rafting, paleocurrent strength, and paleoproductivity in the Bering Sea.

## Hemipelagic deposition

282

283

284

285

286

287

288

289

290

291

292

293

294

295

296

297

298

299

300

301

Deposits on the Bering shelf are derived from various continental sources, and transported to the shelf by several agents, including wind, rivers, and ice (Asahara et al. 2012; Nagashima et al. 2012; Naidu and Mowatt 1983; Nelson 1982; Wang et al. 2016). Accordingly, shelf sediments comprise a broad range of size classes, from clay to coarse sand, gravel, and infrequently, cobbles (>64 mm) (Table 1). Mean grain size on the Bering shelf is a function of the energy of the depositional environment, and generally decreases with increasing depth and distance from the shore (Richwine et al. 2018; Sharma 1972, 1975). Downcore variations in grain size may be linked to a range of processes that operate in deep water to erode, transport and deposit sediments, including gravity-driven, current-driven, and vertical settling processes, each of which produce a distinctive type of deposit or sediment facies. In general, sediments at the three core sites fit the definition of a hemipelagic facies. Hemipelagites are fine-grained (mean 5-35 μm), poorly sorted deposits that comprise a mix of biogenic (>10%) and terrigenous and/or volcanogenic material (>10%), in which at least 40% of the terrigenous fraction is silt-sized or larger (Stow et al. 1998). Hemipelagic sediments are further characterized by a wide range of grain size classes, and typically have a multimodal distribution (Stow and Smillie 2020). Hemipelagites are typical of outer shelf and slope settings and are deposited by a combination of vertical settling and very slow lateral advection in a low energy environment (Stow et al. 1998). Hemipelagic deposition is a continuous process that occurs under more or less steady state conditions, although sedimentation rates may vary in response to changes in biogenic and terrigenous inputs (Stow and Smillie 2020). As such, undisturbed (hemi)pelagic deposits are ideal candidates for paleoceanographic studies.

302

303

304

305

306

307

#### **Indicators of sediment transport**

Shelf sediments may be transported beyond the shelf-slope break by various processes, including bottom currents, downslope transport (e.g., debris flows, turbidity flows), and ice rafting. The characteristics of these slope deposits are inherited from the source material but may be somewhat altered by the processes occurring during transport and deposition (McLaren 1981). Sediment grain size may be

influenced by multiple transport mechanisms and/or flow modifications; some studies (e.g., Murdmaa et al. 2019) have used end-member modeling of grain size distributions to distinguish sedimentation processes, but that is beyond the scope of this study.

Sediments from our study sites on the Bering slope contain a mix of different size classes, and have a multimodal distribution, reflecting the diverse sediment inputs to the shelf. In addition, the sediments are poorly to very poorly sorted. The grain size distribution suggests that icebergs and/or sea ice are likely transport agents, because ice-rafted debris (IRD) typically consists of poorly sorted sediment with a wide range of grain sizes (Krissek et al. 1985; Lisitzin 2002; Reimnitz et al. 1998; Sakamoto et al. 2005; von Huene et al. 1973). In addition, we cannot ignore the role of current action, which may transport finer grains as suspended load, and coarser grains via bed load across the seafloor (Stow and Smillie 2020), however, bottom currents rarely transport particles >63 µm (Masson et al. 2004; McCave and Hall 2006). Turbidity currents can transport much coarser material, and in fact, are one of the most important ways by which fine-, medium-, and coarse-grained materials are transported from the shelf into deeper water (Stow and Smillie 2020). However, the characteristic features of turbidite deposits (e.g., moderate to good sorting, normal grading, abrupt changes in grain size, and clear erosive surfaces) are not apparent at any of our core sites.

The skewness of a deposit reflects the ability of the transport agent to selectively remove finer or coarser material. A symmetrical or near-symmetrical skewness may indicate a low-energy environment, whereas high skewness values may indicate a large amount of sediment reworking (Cadigan 1961). Sediments may become fine-skewed due to the removal of fines by winnowing, or through selective deposition of grains in transport. Alternatively, they may become coarse-skewed, due to total deposition of the transported sediment (McLaren 1981; Martins 2003). In general, Bering Sea sediments are either near symmetrical, or slightly coarse-skewed (text-fig. 5), suggesting a relatively low energy depositional environment. At sites U1345 and U1343, however, there is an interval from ~408-400 ka where sediments become more fine-skewed (text-fig. 5), which may reflect a change in energy conditions at this time.

Several factors complicate the use of skewness as a proxy for sediment transport processes.

Firstly, skewness values often reflect the grain size characteristics of the source material, rather than the energy of the transport medium (Andrews and van der Lingen 1969; McLaren 1981). Secondly, skewness can result from subequal mixing of different grain size populations in a multimodal distribution (Folk and Ward 1957). Lastly, skewness is a metric best suited to well sorted, unimodal sediments; indeed, the primary application of skewness in grain size studies seems to be in distinguishing between adjacent deposits of well sorted sediments, such as dune sands and beach sands (e.g., Friedman 1961, 1979; Kaspar-Zubillaga and Carranza-Edwards 2005; Lopez et al. 2020; Martins 2003; McLaren 1981; Sevon 1965). Cadigan (1961) showed that asymmetry in poorly sorted sediments produces much lower skewness values than in well-sorted sediments. As sediments from the Bering Sea are both poorly sorted and multimodal, skewness may have a limited application in this study.

#### **Contourites**

At sites U1345 and U1343, there is a coarse interval centered on 403.5 ka (text-figs. 5, 6). Sediments from this interval do not match the signature of hemipelagic deposits, and thus indicate a change in sediment facies. Based on grain size distribution and sedimentary structures identified from core photos (irregular sandy lenses, sand mottles, sand layers, and indistinct dark laminations) we suggest that this anomalous interval may be a contourite, a sediment deposited or reworked by the persistent action of bottom currents. Specifically, sediments from this interval fit the description of a fine-grained, muddy or silty contourite (Rebesco et al. 2014; Stow and Smillie 2020). Fine-grained contourites are a mix of biogenic and terrigenous sediment, characterized by poor sorting, unimodal distribution, and a bi-gradational unit in the range of 0.5 to 3 m thick (Rebesco et al. 2014; Stow and Smillie 2020). The 'coarse interval' at sites U1345 and U1343 is in fact a ~2 m thick bi-gradational sequence, with a coarsening upward unit (~408 to 403.5 ka) followed by a fining upward unit (403.5 to ~400 ka) (text-fig. 6).

Evidence for a contourite is particularly strong at U1345; samples from the coarsest part of the deposit at this site represent the only unimodal grain size distribution in the entire record. The coarsest deposits at

U1343 are not unimodal, likely due to input of poorly sorted IRD during this interval. Irregular sandy lenses, sand mottles, sand layers, and indistinct dark laminations occur both before and after the bigradational sequence at both sites (text-fig. 6). Typically, lenses of coarser material are one of the few sedimentary structures preserved in contourite facies, due to the pervasive bioturbation associated with contourites (Stow et al. 2002; Stow and Faugères 2008; Stow and Smillie 2020).

Historically, contourite processes have been linked to bottom current dynamics (Gonthier et al. 1984), however, sediment supply is also a major control on the formation of contourite facies (e.g., Michels et al. 2001; Mulder et al. 2013; Rebesco et al. 2014). For example, Mulder et al. (2013) showed that the same facies succession can be derived in one of two ways: either by the selective removal of fine-grained material through winnowing, or from a new supply of coarser grains, which could include material transported from upstream contourite drifts, as well as more remote sources, such as rivers. At high latitudes, the process of ice rafting may provide a further supply of coarse, terrigenous particles. As sediments at sites U1345 and U1343 become more fine-skewed during the contourite, we propose that winnowing is the main control on the development of contourite facies on the Bering slope.

Although evidence for contourite deposits at sites U1345 and U1343 is strong, it is somewhat unusual to find a single contourite facies. Most contourites are formed by the action of bottom currents, which are strongly influenced by thermohaline and wind-induced circulation; as a result, contourite sequences are believed to reflect regular or sub-regular periodicities in mean bottom current velocities, driven by larger-scale changes in oceanic and atmospheric circulation, climate, and sea level (Stow et al. 2002; Stow and Smillie 2020). Stow et al. (2002) calculated periodicities for contourite drifts of terrigenous to mixed composition in various locations, including the Gulf of Cadiz, Rockall Margin, West Shetlands, and Norwegian Margin, and obtained periodicities between 5,000 and 20,000 years. In addition, periodicities of 20,000-40,000 years have been observed in bioclastic contourites, analogous to the Milankovitch cyclicity recognized in many pelagic and hemipelagic deposits, whilst cycles between 20 and 200 ka have been estimated for ancient contourite systems (Hüneke and Stow 2008; Stow and Faugères 2008). It is possible that contourites on the Bering slope have longer periodicities, such as the

100-ka cycle, but we are unable to resolve such periodicities in a ~60,000-year record. No modern contourite deposition has been reported for the Bering Shelf, but Pelto et al. (2018) speculate that contourite deposition may have been happening at Navarin Canyon since the early Holocene, based on abundant sand deposits in core 3JPC (text-fig. 1). Alternatively, bottom currents can also operate as part of upwelling and downwelling systems, up- and down-canyon currents, internal tides and waves, and seafloor polishing and spillover. Such processes may produce isolated examples of contourite facies (Faugères and Stow 2008; Hüneke 2016). The BSC today has velocities of up to 0.033 m/s at 1,000 m depth (Johnson et al. 2004); strengthening of this current due to changing sea level could have been a trigger for contourite deposition.

The presence of contourite sequences raises some concerns about the validity of the existing age models, given that we do not know exactly how the processes responsible for contourite formation might influence sedimentation rates, and the input of older, reworked sediment to the core sites. However, it has been shown that deposition in contourite drifts is mostly continuous, thus enabling good age control (e.g., Mulder et al. 2013; Toucanne et al. 2007; Voelker et al. 2006). There is no evidence for older, reworked material in our deposits; oxygen isotope values of benthic foraminifera from within the contourites are consistent with those from the hemipelagic deposits. Although sedimentation rates may be more variable within the contourite sequences, small-scale variations in sedimentation rates should not affect our interpretation of the core records on orbital or millennial timescales.

#### **Proxy for ice rafting**

Ice rafting is the process by which glaciers and/or sea ice entrain and transport terrigenous and near-shore particles far from land. As the ice melts, it releases the entrained sediment, which settles through the water column, and accumulates on the seafloor (Dowdeswell 2009). Ice rafting is an important mode of sediment transport at high latitudes (Andrews 2000; Dowdeswell 2009; Gilbert 1990; Kennish 2002; Ruddiman 1977), and results in deposits of poorly sorted, coarse-grained siliciclastic material, known as IRD. In reality, the process of ice rafting can transport a large range of particle sizes,

from fine-grained clays, to coarse sands, gravel, and dropstones (e.g., Krissek et al. 1985; Lisitzin 2002; Reimnitz et al. 1998; Sakamoto et al. 2005; von Huene et al. 1973), but we typically examine the coarse fraction in IRD studies, because ice rafting is one of the few mechanisms capable of transporting coarse (sand-sized and larger) grains into the open ocean. Other possible mechanisms include turbidity currents, mass wasting, and volcanic activity. We see no evidence for turbidites at any of the core sites, but it is entirely possible that grain size could be influenced by other forms of downslope transport (Masson et al. 2006). Volcanogenic material, mostly in the form of fine ash, has been identified from visual core descriptions, core images, and smear slide analyses at all three sites (text-figs. 5, 7; Takahashi et al. 2011). Ash is most abundant at Site U1339, due to its proximity to the main volcanic source of the Aleutian Arc and is a more minor component of the sediments at U1345 and U1343 (text-figs. 5, 7; Takahashi et al. 2011). However, there is no consistent relationship between the volume % of coarse terrigenous grains and the presence of ash layers or accessories (text-fig. 7), which suggests that volcanogenic material is not a major control on grain size. Considering that other transport mechanisms can mostly be ruled out, we interpret the bulk of the coarse terrigenous grains as IRD.

IRD is defined as the weight percent, volume percent, or number of terrigenous grains within a given size fraction (Dowdeswell 2009). We recognize that different workers define IRD in different ways; here, we follow St. John (2008) in examining the volume percent of particles in the >150 μm and >250 μm size fractions (text-fig. 7). Regardless of which measure we analyze, IRD is present at all sites throughout almost the entire investigated record. The volume % of grains >150 μm averages 6.3%, 5.5%, and 5.4% at sites U1345, U1343 and U1339, respectively; for the >250 μm size fraction, average values are 4.4%, 3.4%, and 3.6%, although there is considerable downcore variability at all sites (text-fig. 7). The highest volume % of coarse grains at sites U1345 and U1343 falls within the interval that we define as a contourite. In particular, at site U1343, the volume % of grains >250 μm is notably high (22.1%) at 403.39 ka (text-fig. 7). During this interval, we are unable to distinguish between IRD and coarse contourite deposits, based on grain size alone. However, smear slide analysis of the coarsest sample from Site U1343 revealed the presence of very coarse siliciclastic grains, interpreted as IRD (text-fig. 8). In

addition, the grain size distribution of this sample is very poorly sorted and resembles the grain size distribution of sediments from the Sea of Okhotsk that were deposited under melting sea ice (text-fig. 8; Sakamoto et al. 2005). Ice-rafted material is a passive input into fine-grained contourite deposits and is not subsequently reworked to any great extent by bottom currents (Rebesco et al. 2014), therefore, ice rafting may introduce coarser sediments into a fine-grained contourite deposit, independent of the processes acting to form the contourite facies (e.g., Howe et al. 2007; Lucchi and Rebesco 2007).

Overall, the IRD records presented here suggest that iceberg and/or sea ice rafting was an important source of sediment delivery to the Bering slope throughout MIS 11. Distinguishing between iceberg and sea ice rafting processes is critical to understanding the ice rafting history of an area, but it can be hard to distinguish iceberg-rafted debris from sea ice-rafted debris, based on grain size alone (St. John et al. 2015). Although iceberg-rafted material is often considered to be coarser than that transported by sea ice, under certain conditions, both icebergs and sea ice are capable of transporting a comparable fraction of coarse terrigenous material far offshore (e.g., Darby et al. 2011; Darby and Zimmerman 2008; Lisitzin 2002; Mager et al. 2013; Nürnberg et al.,1994; St. John et al. 2015). However, it should be noted that tidewater glaciers are uncommon in the Bering Sea, especially during interglacial periods (Caissie et al. 2016), so it is likely that most of the IRD in our records was transported by sea ice.

#### **Proxy for paleocurrent strength**

The mean size of sortable silt (10-63  $\mu$ m) is used as a proxy for the flow speed of near-bottom currents in the deep ocean, with coarser deposits reflecting higher flow speeds. (McCave et al. 1995, 2017). This particular size fraction is used, because at the upper limit, ocean currents rarely transport grains larger than 63  $\mu$ m (Masson et al. 2004; McCave and Hall 2006), and at the lower limit, particles less than 10  $\mu$ m tend to behave cohesively (McCave et al. 1995; McCave and Hall 2006). However, there are several caveats to be considered when using sortable silt as a paleocurrent proxy, especially in the subarctic. Firstly, the sortable silt proxy should only be used to infer current strength if there is a positive correlation between the mean size of sortable silt ( $\overline{SS}$ ) and the percent sortable silt ( $\overline{SS}$ %), indicating a

current-sorted regime (McCave and Andrews 2019; Roberts et al. 2017). In addition, several studies (e.g., Jonkers et al. 2015; Wu et al. 2018) suggest that the sortable silt proxy is not effective in regions with IRD input, because the input of ice-rafted silt may complicate the interpretation of paleocurrent strength. Lastly, McCave and Hall (2006) caution against using laser particle sizers for paleocurrent reconstructions, due to particle shape-related artifacts, Specifically, the platy shape of clay and fine silt particles in the 10-30 µm range may cause them to be recorded as the same size as coarser equant grains, which tends to enhance medium silt abundance.

To test whether sortable silt is an effective proxy for current strength at our core sites, we examined downcore variations in  $\overline{SS}$  (text-fig. 9), as well as the relationship between  $\overline{SS}$  and SS%. The mean size of sortable silt (calculated for the terrigenous fraction) decreases from north to south, from an average of 28.1 µm at Site U1345, to 26.6 µm at U1343, and 25.5 µm at U1339. At all sites,  $\overline{SS}$  increases following deglaciation, in line with sea level rise and flooding of the Bering Shelf (text-fig. 9). At U1339,  $\overline{SS}$  stays relatively consistent throughout MIS 11, but at sites U1345 and U1343, sortable silt size is more variable, with consistently higher values (>30 µm) from ~407 to 401 ka (text-fig. 9). This increase in  $\overline{SS}$  corresponds to the period of contourite formation, during which time we might reasonably expect to see an increase in current sorting. However, our records suggest the opposite. There is little to no positive correlation between  $\overline{SS}$  and SS% at any of our core sites, and in fact, there is a strong negative correlation ( $R^2 = -.87$ ) during the contouritic interval at Site U1345 (text-fig. 10), likely due to contamination by unsorted IRD. As our records indicate a lack of current sorting (text-fig. 10), we are unable to use sortable silt as a proxy for paleocurrent strength in the Bering Sea.

## **Proxy for paleoproductivity**

Our analyses show that silt is the predominant size class in Bering Sea sediments, and that the volume % of silt-sized grains is greater for bulk than terrigenous samples (Table 1; text-fig. 4). This suggests that the grain size distribution of bulk sediments may be influenced by the abundance of silt-sized biogenic material. In the Bering Sea, diatom frustules are the main component of biogenic

sediments, and most diatom species in our samples fall within the silt-sized fraction. Therefore, biosilica digestion has the effect of reducing the volume % of particles in the silt size class, which in turn can affect median/mean grain size. Aiello and Ravelo (2012) showed that ~40% of variability in the mean grain size of Bering Sea sediments can be explained by variations in the abundance and preservation of diatom valves, and to a lesser extent, sponge spicules, and suggested that mean grain size provides a rough indication of trends in diatom productivity. With this in mind, we examined the relationship between diatom content (referring to the relative % abundance of diatom valves in comparison to other sediment components) and mean grain size in a subset of samples from sites U1345 and U1339 (text-fig. 11). At Site U1339, diatom content explains ~23% of variability in the mean grain size of bulk sediments, whereas at Site U1345, there is virtually no correlation between diatom content and mean grain size (textfig. 11). We postulate that differences between the two sites are linked to differences in sediment composition; sediments at U1339 have a higher diatom content, whilst biogenic material at Site U1345 is heavily diluted by siliciclastic input, so that diatom content has less of an influence on grain size (Aiello and Ravelo 2012; Kanematsu et al. 2013). Our findings differ from those of Aiello and Ravelo (2012), in part because their analyses included sediments from Bowers Ridge in the southern Bering Sea, where sediments are less diluted by terrigenous matter, but not sediments from U1345. It is also possible that diatom content has more of an influence on grain size over glacial-interglacial timescales, and less so at the finer resolution of this study.

489

490

491

492

493

494

495

496

497

498

499

500

501

502

503

504

505

506

507

508

509

510

511

512

513

514

Based on the relationship between diatom content and mean grain size (text-fig. 11), it is clear that diatom content is not a major control on bulk grain size, especially at Site U1345. How else, then, do we account for differences in mean grain size between bulk and terrigenous samples? Smear slide analyses show that there are additional biogenic controls on mean grain size, including the preservation of diatom valves, and the size of diatoms within the assemblage (text-fig. 12). If the diatom valves are poorly preserved, or fragmented, bulk mean grain size is likely to be smaller, because the sample is dominated by clay and/or fine silt-sized diatom fragments, as opposed to larger silt-sized and even sand-sized whole diatom valves. Accordingly, sediment becomes coarser (mean grain size increases) when the

finer-grained biogenic material is dissolved (text-fig. 12a). Conversely, if the diatoms are well-preserved, sediment may become finer after removing biogenic components in the coarse silt range (text-fig. 12b). For similar reasons, the size of diatom valves in the assemblage can also influence the mean grain size of bulk sediments. For example, an assemblage dominated by small pennate diatoms, such as *Neodenticula seminae* (Simonsen and T. Kanaya) Akiba and Yanagisawa 1986, is likely to be finer grained than a sediment containing large, centric diatoms, such as *Coscinodiscus* Ehrenberg species, which can be up to ~200 μm or more in diameter (Sancetta 1987). The degree of coarsening or fining also depends on the grain size distribution of siliciclastic material. In sediments with sub-equal proportions of well-preserved, silt-sized diatoms and silt-sized siliciclastics, for example, we might not expect much difference in mean grain size between the bulk and terrigenous samples. However, if the sediment were comprised of well-preserved, silt-sized diatoms, and abundant silt- to sand-sized siliciclastic material, the mean grain size of the terrigenous fraction is likely to be coarser than that of the bulk sediment.

Aiello and Ravelo (2012) discussed the importance of diatom preservation on the mean grain size of bulk sediments at several sites across the Bering Sea. They found that the mean grain size of bulk sediments was coarser during the Holocene and the Last Interglacial, due to relatively high abundances of well-preserved, whole, silt-sized diatom valves. In contrast, samples from the Last Glacial Maximum contained poorly preserved, fragmented diatoms, and abundant clay-sized particles. Likewise, our smear slide analyses showed more fragmented diatoms, corresponding to a slightly lower mean grain size, during the glacial periods (MIS 12 and 10) within our study timeframe (Table S1).

To summarize, mean grain size is not a direct or straightforward proxy for paleoproductivity, but at the very least, downcore variations in the mean grain size of bulk sediments can be used to infer changes in productivity that occur on glacial-interglacial cycles (Aiello and Ravelo 2012). In addition, when combined with smear slide analyses, grain size records may provide valuable information on changes in diatom abundance, preservation, and assemblage composition.

#### **SUMMARY**

In this study, we aimed to show how grain size parameters, including the volume percent of grains in various size fractions, as well as the statistical measures of mean grain size, sorting, and skewness, can be used to infer past oceanographic conditions at three core sites in the Bering Sea. At all three sites, sediments are a poorly sorted, multimodal mix of siliciclastic and biogenic sediments, with minor volcanogenic input. The southernmost site, U1339, has more biogenic and volcanogenic grains, whilst Site U1345, located on the northern slope, has the most siliciclastic input. Sediments at Site U1343 represent an intermediate composition between the other two sites.

Sediments in the Bering Sea can primarily be classified as hemipelagites, making them ideal deposits for paleoenvironmental reconstructions. There is no evidence for turbidite deposition at any site; however, there is strong evidence for contourite facies deposited between ~408-400 ka at sites U1345 and U1343. Contourites are associated with sediment reworking through the action of bottom currents, and there is evidence for winnowing of finer sediments during this interval, which may complicate paleoclimate interpretations.

The prevalence of very coarse (>150 um) grains throughout all three records indicates that ice rafting is a consistent source of sediment transport to the Bering slope, but we are unable to distinguish between iceberg and sea ice rafting processes, based on grain size alone. In general, mean grain size can be used to infer productivity on glacial-interglacial timescales, however, both the size and the preservation of diatom valves also exert a control on mean grain size. Finally, the mean size of sortable silt is not a valid proxy for bottom current strength in the Bering Sea, most likely because the input of icerafted silt confounds the sortable silt signal.

## DATA AVAILABILITY

Datasets used in this study are publicly available in the NSF Arctic Data Center repository at <a href="https://arcticdata.io/catalog/view/doi%3A10.18739%2FA2H12V839">https://arcticdata.io/catalog/view/doi%3A10.18739%2FA2H12V839</a> (Thompson and Caissie 2021). Supplemental Table S1 shows diatom content (relative % abundance) from smear slide counts at sites

U1345 and U1339. It can be found at: <a href="https://www.micropress.org/microaccess/stratigraphy/issue">https://www.micropress.org/microaccess/stratigraphy/issue</a>, an open-source online repository hosted by Micropaleontology Press.

## **ACKNOWLEDGEMENTS**

We thank Kate Staebell for helping to analyze grain size data and Mark Mathison for technical assistance with the Mastersizer. We also thank our reviewers, Jason Chaytor, Thomas Cronin, and Laura Gemery, for their careful reading of our manuscript, and their insightful comments. This work was partially funded by the National Science Foundation Office of Polar Programs under Grant No. 1903724/2110923. Any use of trade, firm, or product names is for descriptive purposes only and does not imply endorsement by the U.S. Government.

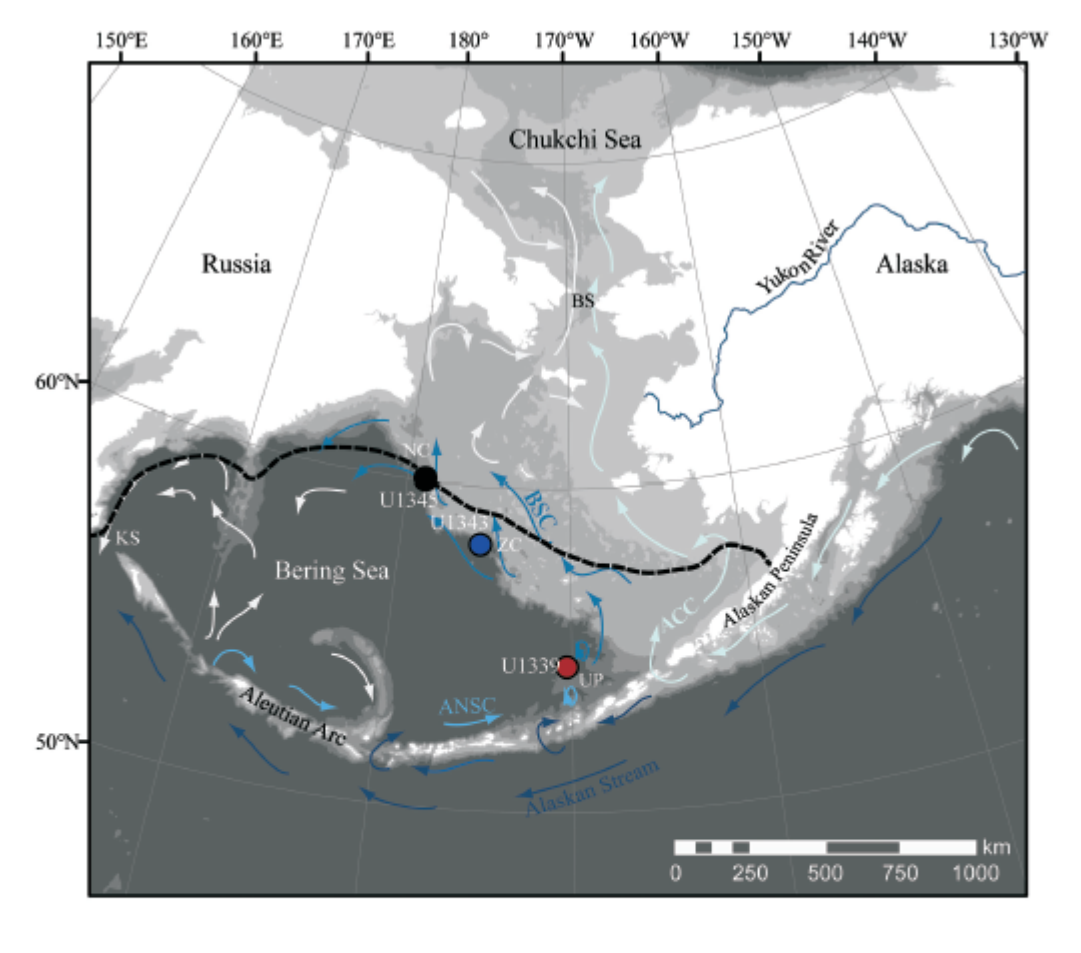
## **TABLES**

TABLE 1
Grain size averages for bulk (top) and terrigenous (bottom) sediments from IODP Sites U1345, U1343 and U1339.

Bulk sediment											
Site	n	Median (μm)	Mean (μm)	Sorting	Skewness	% Clay (<2 μm)	% Silt (2-63 μm)	% Sand (63-2000 μm)	Gravel (>2000 μm)		
U1345	97	20.8	20.3	2.9	-0.01	1.1	84.2	14.6	0.1		
U1343	239	17.3	16.8	3.7	-0.03	5.8	78.7	14.9	0.6		
U1339	297	19.7	19.1	3.6	-0.05	4.3	77.5	18.1	0.1		
Terrigenous sediment											
Site	n	Median (μm)	Mean (μm)	Sorting	Skewness	% Clay (<2 μm)	% Silt (2-63 μm)	% Sand (63-2000 μm)	Gravel (>2000 μm)		
U1345	89	21.7	20.7	4.8	-0.02	6.2	71.9	20.2	1.4		
U1343	242	17.4	17.4	4.4	0.02	7.3	73.9	18	0.8		
U1339	290	12.6	13.6	4.8	0.11	9.6	74.8	14.9	0.7		

Table 1. Grain size averages for bulk (top) and terrigenous (bottom) sediments from IODP Sites U1345, U1343, and U1339.

#### **FIGURES**



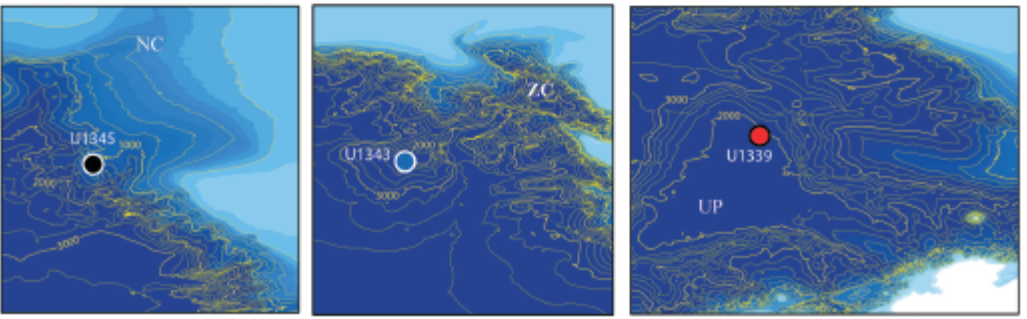


Figure 1. Map of Beringia, showing place names, bathymetric features, and core sites referred to in the text. The black dashed line shows the maximum extent of sea ice today (median over the period 1979-2013) (Cavalieri et al. 1996). Currents are modified from Stabeno et al. (1999) and are depicted with light grey arrows except for Alaska Coastal Current (ACC; light blue arrows), Alaskan Stream (dark blue arrows), Aleutian North Slope Current (ANSC; bright blue arrows), and Bering Slope Current (BSC; blue arrows). Other abbreviations include: Bering Strait (BS), Kamchatka Strait (KS), Navarin Canyon (NC), Zhemchug Canyon (ZC), and Umnak Plateau (UP). Grey bathymetric shading changes value at -50 m

(Bering Strait sill depth), -250 m (shelf/slope break), -1000 m, and -2000 m. Inset maps show the location of each IODP core site at high resolution (Base map from NOAA 2009; inset base maps modified from Zimmerman and Prescott 2018). The contour interval is 200 m.

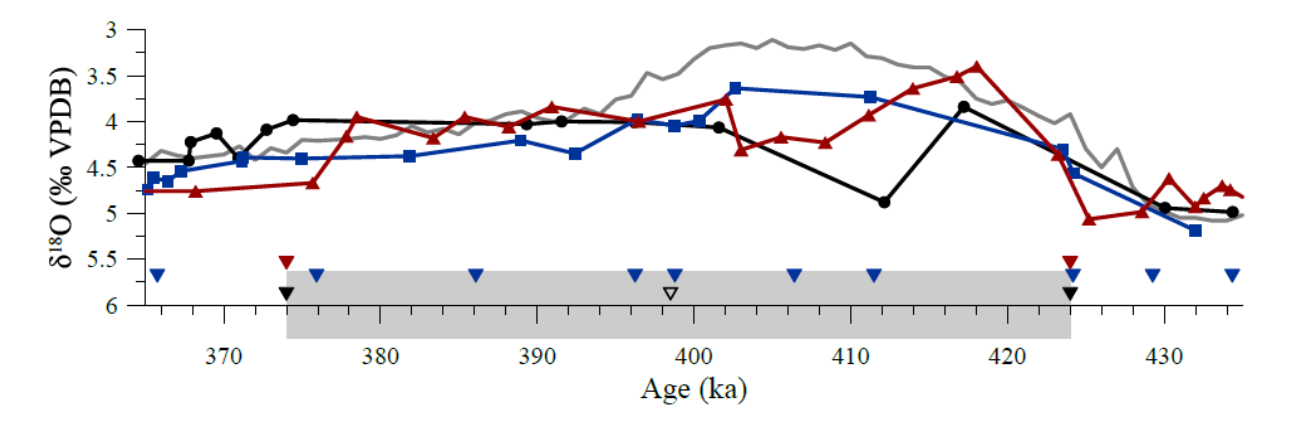


Figure 2. Benthic foraminiferal  $\delta^{18}O$  values for IODP sites U1345 (black; Cook et al. 2016), U1343 (blue; Asahi et al. 2016) and U1339 (red; Cook et al. 2016) compared to the LR04 stack (grey; Lisiecki and Raymo 2005). Inverted triangles show tie points between Bering Sea  $\delta^{18}O$  (filled) and magnetic susceptibility (open) records and the global stack. The grey bar shows the duration of MIS 11.

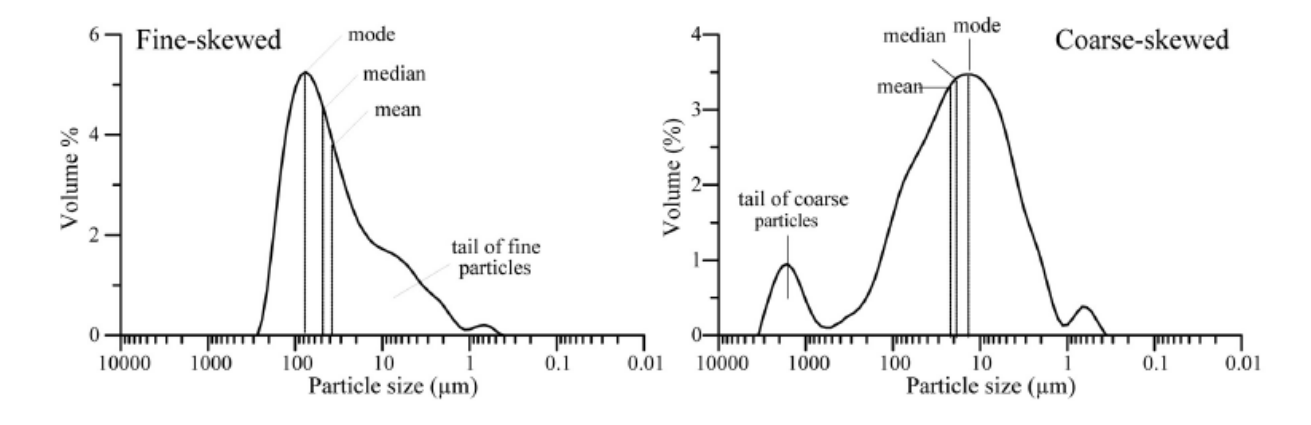


Figure 3. Examples of fine-skewed (U1343A 12H-5 78 cm) and coarse-skewed (U1343C 12H-3 55 cm) samples. Note that the x-axis is reversed to follow convention.

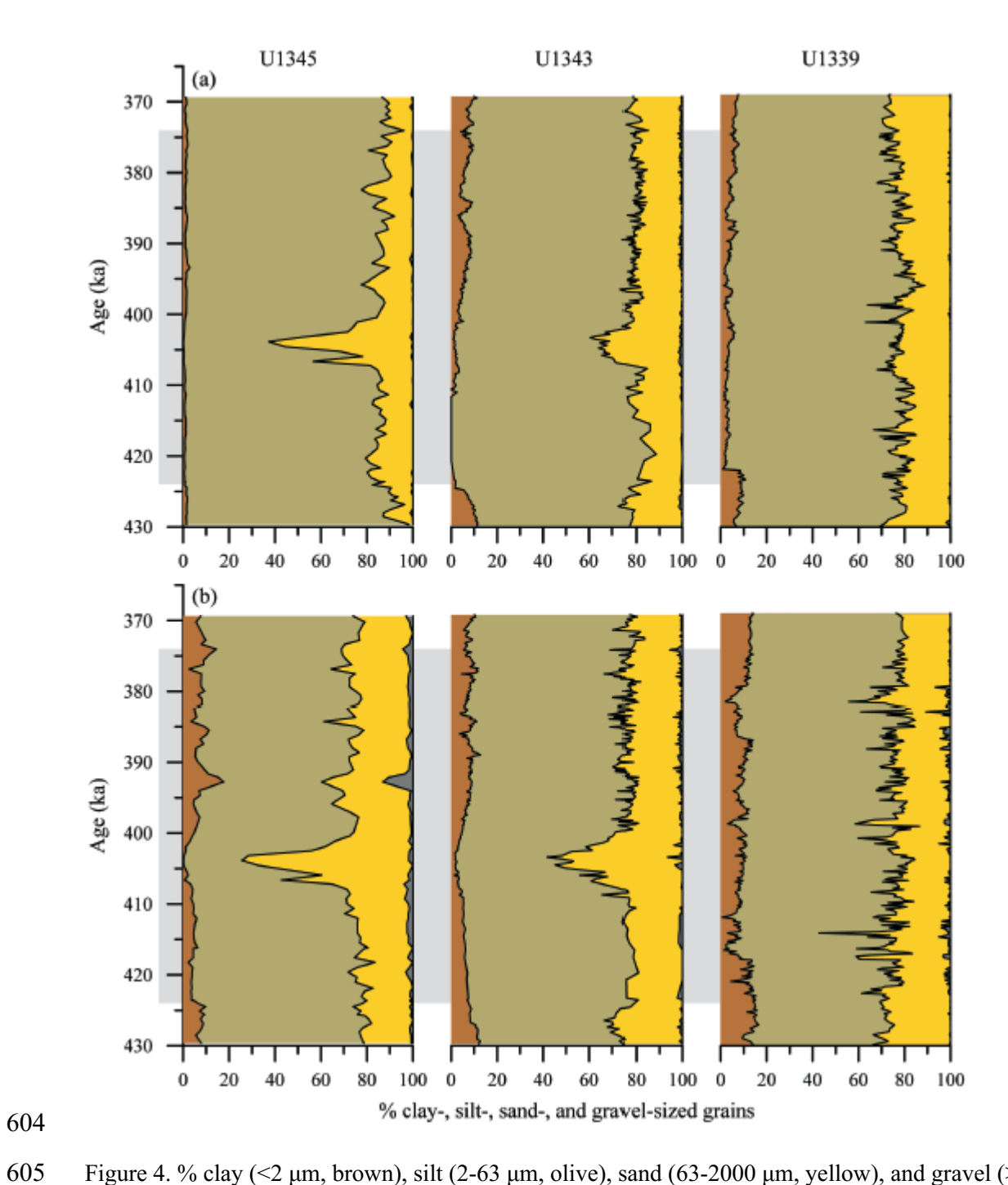


Figure 4. % clay ( $<2~\mu m$ , brown), silt (2-63  $\mu m$ , olive), sand (63-2000  $\mu m$ , yellow), and gravel ( $>2000~\mu m$ , grey) sized grains for (a) bulk and (b) terrigenous sediments at IODP sites U1345, U1343 and U1339. The grey panels show the duration of MIS 11.

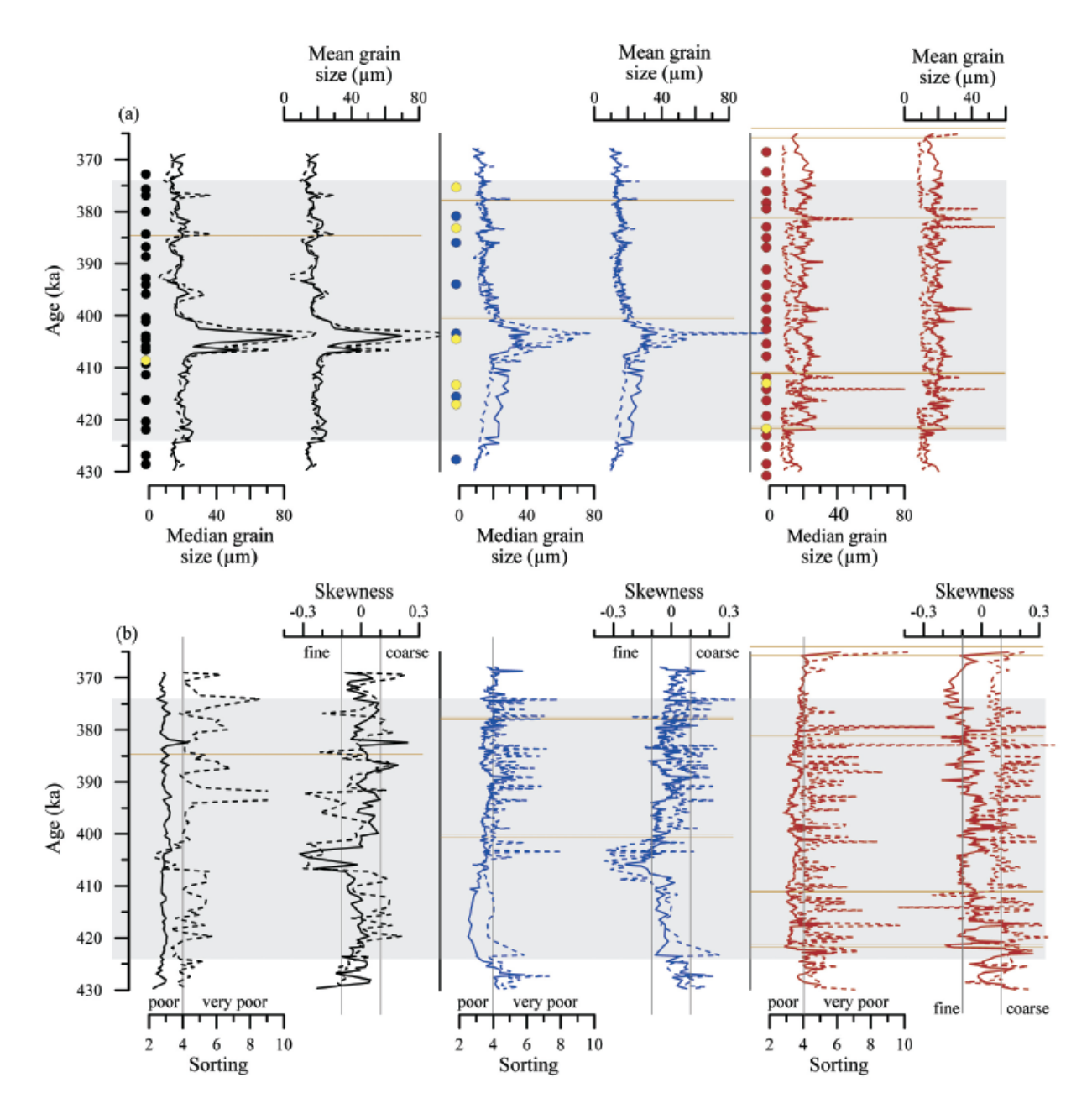


Figure 5. (a) Downcore variations in median and mean grain size for bulk (solid line) and terrigenous (dashed line) sediments from Bering Sea core sites U1345 (black), U1343 (blue), and U1339 (red). Dots indicate the stratigraphic position of smear slide samples; black, blue, and red dots are from this study, yellow dots are smear slides from Takahashi et al. (2011). (b) Downcore variations in sorting and skewness for bulk (solid line) and terrigenous (dashed line) sediments from Bering Sea core sites U1345 (black), U1343 (blue), and U1339 (red). Sorting and skewness values are related to descriptive terms for sorting (poorly sorted [2-4]; very poorly sorted [4-16]) and skewness (symmetrical [-0.1 to 0.1]; fine

skewed [-0.3 to -0.1]; coarse skewed [0.1 to 0.3]) after Folk and Ward (1957). Brown bars show ash layers/accessories, and the grey panels shows the duration of MIS 11.

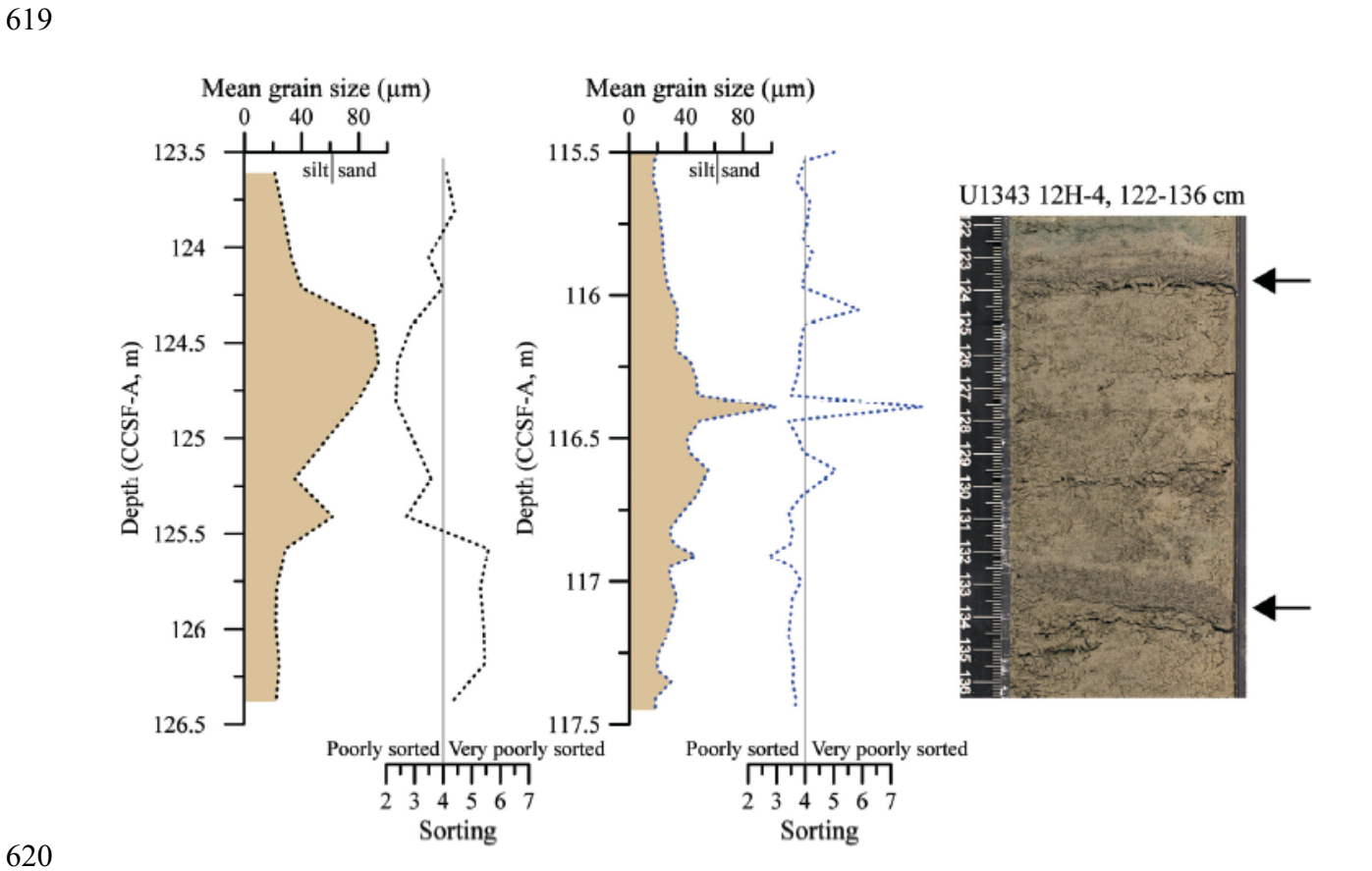


Figure 6. Grain size distribution (mean grain size and sorting) for the contouritic intervals at sites U1345 and U1343. Note that this figure is scaled by depth, not age. The core image shows an example of a sand lens from U1343 but is not scaled the same as the plot.

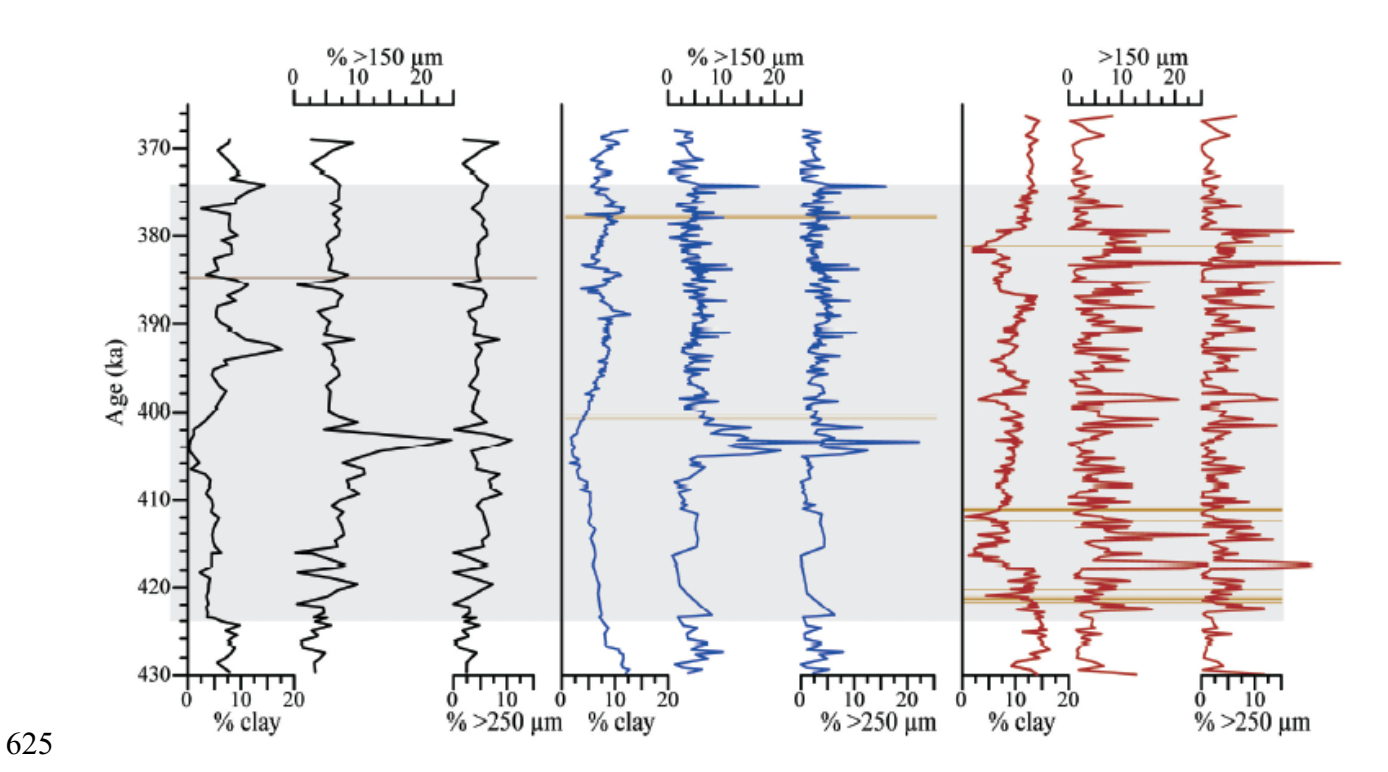


Figure 7. Percent terrigenous clay-sized grains, and % terrigenous grains in the  $>150 \mu m$ , and  $>250 \mu m$  size fractions, for sites U1345 (black), U1343 (blue), and U1339 (red). Brown bars depict ash layers and accessories, and the grey panel shows the duration of MIS 11.

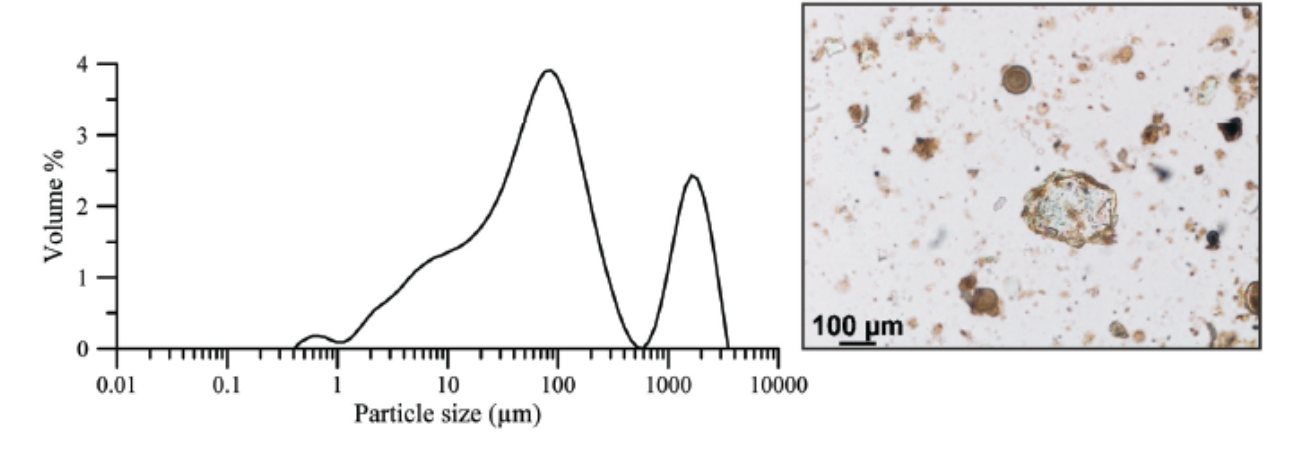


Figure 8. Grain size distribution plot and light microscope image of IRD (magnification 100x) from Site U1343 (12H-5 41-42 cm, 403.4 ka).

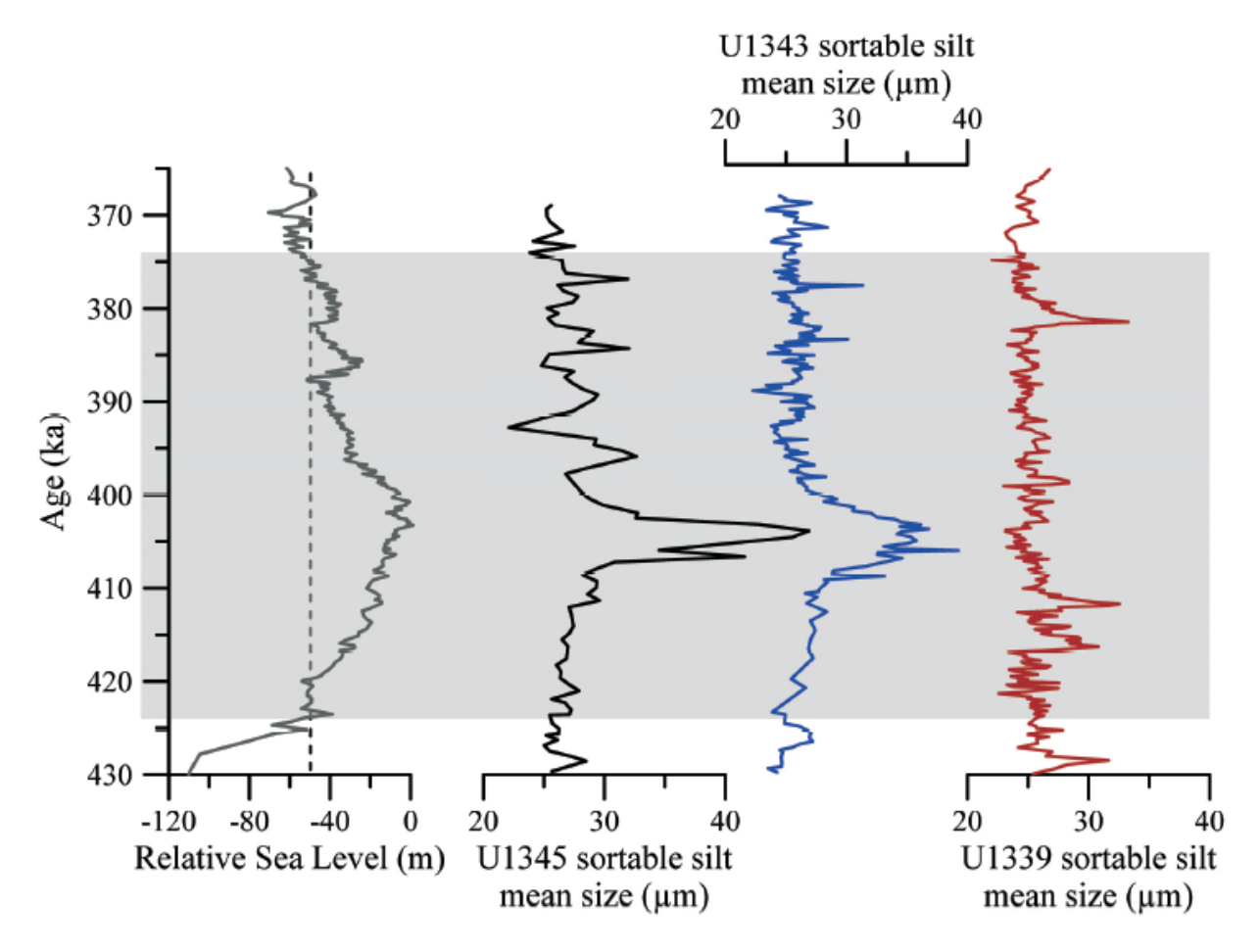


Figure 9. Mean size sortable silt (10-63  $\mu$ m) at IODP sites U1345 (black), U1343 (blue), and U1339 (red), compared to relative sea level (Rohling et al. 2010). The dashed line represents the Bering Strait sill depth (-50 m). The grey panel shows the duration of MIS 11.

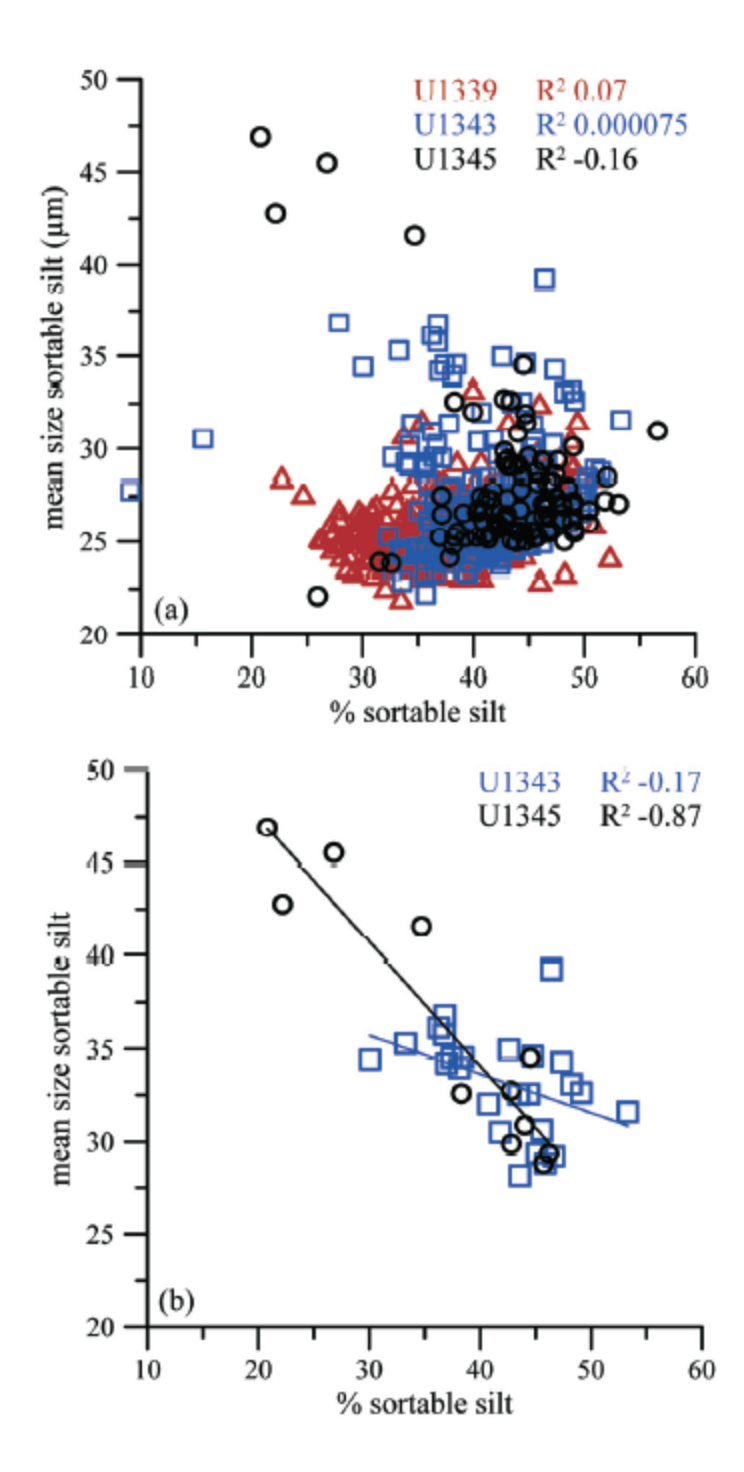
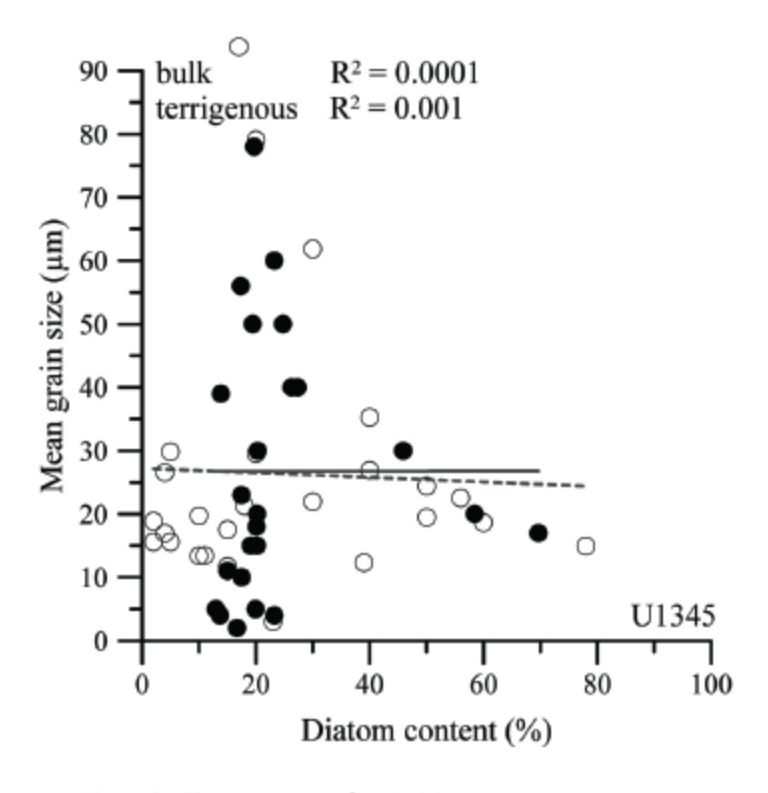


Figure 10. Cross-plots of mean size sortable silt versus % sortable silt for (a) sites U1345 (black), U1343 (blue), and U1339 (red), and (b) contourite deposits from sites U1345 (black) and U1343 (blue).



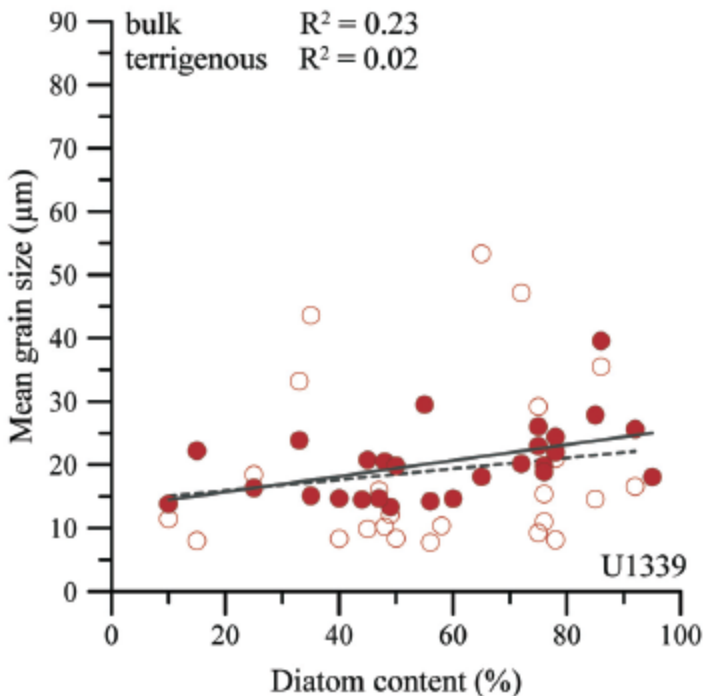


Figure 11. Percent diatoms from smear slide analysis versus mean grain size before (closed circles) and after (open circles) biosilica digestion for sites U1345 (black) and U1339 (red).

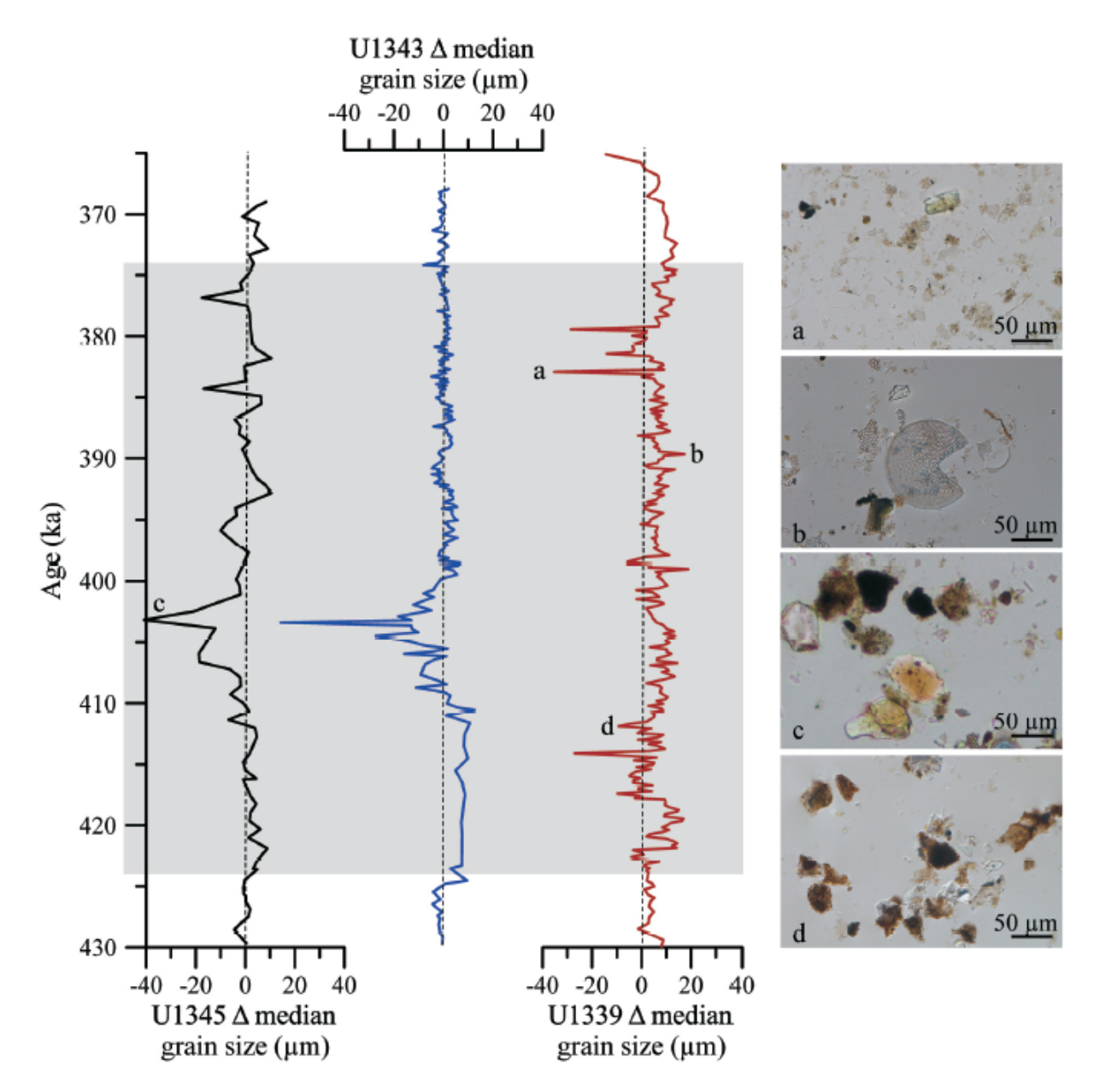


Figure 12. Difference in mean grain size between the two sets of samples (bulk minus terrigenous) at sites U1345 (black), U1343 (blue) and U1339 (red). Positive values indicate fining of sediment, negative values indicate coarsening. Letters on the plot correspond to microscope images, which relate changes in sediment grain size to sediment composition. a. Coarsening, due to poorly preserved (fragmented) diatoms; b. Fining, due to the presence of coarse silt- and sand-sized diatoms; c. Coarsening, due to the presence of coarse silt to sand-sized siliciclastic minerals; and d. Coarsening, due to the combined effects of low diatom content and high volcanogenic input. The grey panel shows the duration of MIS 11.

# 654 SUPPLEMENTAL MATERIALS

Table S1. Diatom content (relative % abundance) from smear slide counts at sites U1345 and U1339.

	Depth (CCSF-A	Age	
Sample	(m))	(ka)	Diatom %
U1339C 10H-4 55 cm	97.51	368.53	10
U1339C 10H-4 125 cm	98.21	372.40	15
U1339C 10H-5 60 cm	99.06	376.07	40
U1339C 10H-5 120 cm	99.66	378.30	45
U1339D 11H-3 10 cm	99.97	379.44	35
U1339D 11H-3 104 cm	100.91	382.93	65
U1339D 11H-4 34 cm	101.48	385.04	76
U1339D 11H-4 84 cm	101.98	386.89	56
U1339D 11H-5 9 cm	102.73	389.67	48
U1339D 11H-5 128 cm	103.92	394.07	78
U1339D 11H-6 44 cm	104.58	396.51	58
U1339D 11H-6 103 cm	105.17	398.70	86
U1339D 11H-7 23 cm	105.82	401.11	55
U1339C 11H-2 105 cm	106.23	402.63	60
U1339C 11H-3 36 cm	106.98	405.41	76
U1339C 11H-3 101 cm	107.63	407.81	85
U1339C 11H-4 61 cm	108.73	411.89	33
U1339C 11H-4 121 cm	109.33	414.11	72
U1339C 11H-5 30 cm	109.92	416.30	75
U1339D 12H-3 10 cm	110.72	419.26	92
U1339D 12H-3 80 cm	111.42	421.85	78
U1339D 12H-3 110 cm	111.62	422.59	25
U1339D 12H-4 15 cm	112.27	425.25	49
U1339D 12H-4 85 cm	112.97	428.48	47
U1339D 12H-4 135 cm	113.47	430.78	50
U1345A 12H-4 66 cm	112.94	369.00	10
U1345A 12H-5 112 cm	114.84	372.82	15
U1345A 12H-6 66 cm	115.88	375.65	5
U1345A 12H-6 105 cm	116.27	376.86	5
U1345A 12H-7 55 cm	117.27	379.96	11
U1345C 12H-5 64 cm	118.67	384.30	20
U1345C 12H-5 144 cm	119.47	386.78	4
U1345C 12H-6 56 cm	120.07	388.64	15
U1345A 13H-2 42 cm	121.41	392.79	23
U1345A 13H-2 82 cm	121.81	394.03	10

U1345A 13H-2 142 cm	122.41	395.89	4
U1345A 13H-3 112 cm	123.61	400.41	18
U1345A 13H-3 132 cm	123.81	401.10	40
U1345A 13H-4 62 cm	124.61	403.86	17
U1345A 13H-4 82 cm	124.81	404.55	20
U1345A 13H-4 122 cm	125.21	405.93	40
U1345A 13H-4 142 cm	125.41	406.62	30
U1345A 13H-5 72 cm	126.18	409.28	50
U1345A 13H-5 132 cm	126.78	411.35	56
U1345A 13H-6 122 cm	128.18	416.18	78
U1345A 13H-7 92 cm	129.38	420.32	50
U1345A 13H-CC 2 cm	129.84	421.91	60
U1345D 13H-5 10 cm	130.77	424.05	2
U1345A 14H-2 42 cm	131.71	426.86	39
U1345A 14H-2 99 cm	132.28	428.55	2

- 658659 REFERENCES
- AIELLO, I. W. and RAVELO, A. C., 2012. Evolution of marine sedimentation in the Bering Sea since
- 661 the Pliocene. *Geosphere*, 8 (6): 1231-1253.
- ANDREWS, J. T., 2000. Icebergs and iceberg rafted detritus (IRD) in the North Atlantic: facts and
- 663 assumptions. *Oceanography*, 13 (3): 100-108.
- ANDREWS, J. T. and PRINCIPATO, S. M., 2002. Grain-size characteristics and provenance of ice-
- proximal glacial marine sediments. In: Dowdeswell, J. D. and O'Cofaigh, C., Eds., Glacier-influenced
- sedimentation on high-latitude continental margins, Geological Society of London Special Publication,
- 667 203: 305-324.
- ANDREWS, P. B. and VAN DER LINGEN, G. J., 1969. Environmentally significant sedimentologic
- characteristics of beach sands. New Zealand Journal of Geology and Geophysics, 12 (1): 119-137.
- 670 ASAHARA, Y., TAKEUCHI, F., NAGASHIMA, K., HARADA, N., YAMAMOTO, K., OGURI, K. and
- TADAI, O., 2012. Provenance of terrigenous detritus of the surface sediments in the Bering and Chukchi
- Seas as derived from Sr and Nd isotopes: implications for recent climate change in the Arctic regions.
- *Deep Sea Research Part II: Topical Studies in Oceanography*, 61-64: 155-171.
- ASAHI, H., KENDER, S., IKEHARA, M., SAKAMOTO, T., TAKAHASHI, K., RAVELO, A. C.,
- ALVAREZ ZARIKIAN, A. C., KHIM, B. K. and LENG, M. J., 2016. Orbital-scale benthic foraminiferal
- oxygen isotope stratigraphy at the northern Bering Sea Slope Site U1343 (IODP Expedition 323) and its
- Pleistocene paleoceanographic significance. Deep Sea Research Part II: Topical Studies in
- 678 *Oceanography*, 125-126: 66-83.
- 679 BEN-AVRAHAM, Z. and COOPER, A. K., 1981. Early evolution of the Bering Sea collision of oceanic
- rises and North Pacific subduction zones. Geological Society of America Bulletin, 92 (7): 485-495.
- BERGER, A. and LOUTRE, M. F., 2002. An exceptionally long interglacial ahead? *Science*, 297 (5585):
- 682 1287-1288.

- BLOTT, S. J. and PYE, K., 2001. GRADISTAT: A grain size distribution and statistics package for the
- analysis of unconsolidated sediments. Earth Surface Processes and Landforms, 26: 1237-1248.
- BOWEN, D. Q., 2010. Sea level ~400,000 years ago (MIS 11): analogue for present and future sea-level?
- 686 *Climate of the Past*, 6: 19-29.
- 687 BRICEÑO ZULUAGA, F., SIFEDDINE, A., CAQUINEAU, S., CARDICH, J., SALVATTECI, R.,
- 688 GUTIÉRREZ, D., ORTLIEB, L., VELAZCO, F., BOUCHER, H. and MACHADO, C., 2016.
- Terrigenous material supply to the Peruvian central continental shelf (Pisco, 14° S) during the last 1000
- 690 years: paleoclimatic implications. *Climate of the Past*, 12: 787-798.
- BROWN, Z. W. and ARRIGO, K. R., 2012. Contrasting trends in sea ice and primary production in the
- 692 Bering Sea and Arctic Ocean. *ICES Journal of Marine Science*, 69: 1180-1193.
- BROWN, Z. W. and ARRIGO, K. R., 2013. Sea ice impacts on spring bloom dynamics and net primary
- 694 production in the Eastern Bering Sea. *Journal of Geophysical Research: Oceans*, 118: 43-62.
- 695 CADIGAN, R. A., 1961. Geologic interpretation of grain-size distribution measurements of Colorado
- 696 Plateau sedimentary rocks. *The Journal of Geology*, 69 (2): 121-144.
- 697 CAISSIE, B. E., BRIGHAM-GRETTE, J., COOK, M. S. and COLMENERO-HIDALGO, E., 2016.
- Bering Sea surface water conditions during Marine Isotope Stages 12 to 10 at Navarin Canyon (IODP site
- 699 U1345). Climate of the Past, 12: 1739-1763.
- 700 CAISSIE, B. E., BRIGHAM-GRETTE, J., LAWRENCE, K. T., HERBERT, T. D. and COOK, M. S.,
- 701 2010. Last Glacial Maximum to Holocene sea surface conditions at Umnak Plateau, Bering Sea, as
- 702 inferred from diatom, alkenone, and stable isotope records. *Paleoceanography*, 25 (1):
- 703 https://doi.org/10.1029/2008PA001671.
- CARLIN, J., ADDISON, J., WAGNER, A., SCHWARTZ, V., HAYWARD, J. and SEVERIN, V., 2019.
- Variability in shelf sedimentation in response to fluvial sediment supply and coastal erosion over the past
- 706 1,000 years in Monterey Bay, CA, United States. Frontiers in Earth Science, 7:
- 707 https://doi.org/10.3389/feart.2019.00113.
- 708 CARTER, R. M., LARCOMBE, P., DYE, J. E., GAGAN, M. K. and JOHNSON, D. P., 2009.

- 709 Long-shelf sediment transport and storm-bed formation by Cyclone Winifred, central Great Barrier Reef,
- 710 Australia. *Marine Geology*, 267 (3): 101-113.
- 711 COOK, M., KEIGWIN, L. and SANCETTA, C., 2005. The deglacial history of surface and intermediate
- water of the Bering Sea. Deep Sea Research Part II: Topical Studies in Oceanography, 52 (16-18): 2163-
- 713 2173.
- 714 COOK, M., RAVELO, A., MIX, A., NESBITT, I. and MILLER, N., 2016. Tracing subarctic Pacific
- water masses with benthic foraminiferal stable isotopes during the LGM and late Pleistocene. *Deep Sea*
- 716 Research Part II: Topical Studies in Oceanography, 125-126: 84-95.
- 717 CRONAN, D.S., 1972. Skewness and kurtosis in polymodal sediments from the Irish Sea. *Journal of*
- 718 Sedimentary Research, 42 (1): 102-106.
- 719 CRONIN, T. M., KELLER, K. J., FARMER, J. R., SCHALLER, M. F., O'REGAN, M., POIRIER, R.,
- 720 COXALL, H., DWYER, G. S., BAUCH, H., KINDSTEDT, I. G., JAKOBSSON, M., MARZEN, R. and
- SANTIN, E., 2019. Interglacial paleoclimate in the Arctic. Paleoceanography and Paleoclimatology, 34
- 722 (12): 1959-1979.
- 723 DANIELSON, S., HEDSTROM, K., AAGAARD, K., WEINGARTNER, T. and CURCHITSER, E.,
- 724 2012. Wind-induced reorganization of the Bering shelf circulation. *Geophysical Research Letters*, 39 (8):
- 725 https://doi.org/10.1029/2012GL051231.
- DARBY, D. A., MYERS, W. B., JAKOBSSON, M. and RIGOR, I., 2011. Modern dirty sea ice
- characteristics and sources: the role of anchor ice. *Journal of Geophysical Research*, 116:
- 728 https://doi.org/10.1029/2010JC006675.
- DARBY, D. A. and ZIMMERMAN, P., 2008. Ice-rafted detritus events in the Arctic during the last
- glacial interval, and the timing of the Innuitian and Laurentide ice sheet calving events. *Polar Research*,
- 731 27 (2): 114-127.
- 732 DEGELLEKE, L., HILL, P., KIENAST, M. and PIPER, D., 2013. Sediment dynamics during Heinrich
- event H1 inferred from grain size. *Marine Geology*, 336: 160-169.

- 734 DOWDESWELL, J. A., 2009. Ice-Rafted Debris (IRD). In: Gornitz, V., Ed., Encyclopedia of
- 735 Paleoclimatology and Ancient Environments, doi:10.1007/978-1-4020-4411-3 113.
- DROXLER, A. W. and FARRELL, J. W., 2000. Marine isotope stage 11 (MIS 11): new insights for a
- warm future. Global Planetary Change, 24 (1): 1-5.
- 738 DUTTON, A., CARLSON, A. E., LONG, A. J., MILNE, G. A., CLARK, P. U., DECONTO, R.,
- HORTON, B. P., RAHMSTORF, S. and RAYMO, M. E., 2015. Sea-level rise due to polar ice-sheet mass
- 740 loss during past warm periods. *Science*, 349: doi:10.1126/science.aaa4019.
- 741 FAUGÈRES, J.-C. and STOW, D. A. V., 2008. Contourite drifts: nature, evolution and controls. In:
- Rebesco, M. and Camerlenghi, A., Eds., Contourites: developments in sedimentology, 60: 257-
- 743 288. Boston: Elsevier.
- FOLK, R. L. and WARD W. C., 1957. Brazos River bar: a study in the significance of grain size
- parameters. *Journal of Sedimentary Research*, 27 (1): 3-26.
- FRIEDMAN, G. M., 1961. Distinction between dune, beach, and river sands from their textural
- 747 characteristics. *Journal of Sedimentary Research*, 31 (4): 514-529.
- FRIEDMAN, G. M., 1979. Differences in size distributions of populations of particles among sands of
- various origins. Sedimentology, 26: 3-32.
- 750 FRIEDMAN, G. M. and SANDERS, J. E., 1978. *Principles of sedimentology*, New York: Wiley, 792 pp.
- 751 GILBERT, R., 1990. Rafting in glacimarine environments. In: Dowdeswell, J. A. and Scourse, J. D., Eds.,
- 752 Glacimarine environments: processes and sediments, Geological Society of London Special Publication,
- 753 53: 105-120.
- GOLDFINGER, C., GALER, S., BEESON, J., HAMILTON, T., BLACK, B., ROMSOS, C., PATTON,
- J., HANS NELSON, C., HAUSMANN, R. and MOREY, A., 2017. The importance of site selection,
- sediment supply, and hydrodynamics: a case study of submarine paleoseismology on the northern
- 757 Cascadia margin, Washington USA. *Marine Geology*, 384: 4-46.

- 758 GONTHIER, E., FAUGÈRES, J. -C. and STOW, D. A. V., 1984. Contourite facies of the Faro Drift, Gulf
- of Cadiz. In: Stow, D. A. V. and Piper, D. J. W., Eds., Fine grained sediments, deep-water processes and
- 760 facies, Geological Society of London Special Publication, 15: 275-291.
- HOFFMAN, S. S., DALSING, R. E. and MURPHY, S. C., 2019. Sortable silt records of intermediate-
- depth circulation and sedimentation in the Southwest Labrador Sea since the Last Glacial Maximum.
- 763 *Quaternary Science Reviews*, 206: 99-110.
- HOLZ, C., STUUT, J. -B., HENRICH, R. and MEGGERS, H., 2007. Variability in terrigenous
- sedimentation processes off northwest Africa and its relation to climate changes: inferences from grain-
- size distributions of a Holocene marine sediment record. Sedimentary Geology, 202 (3): 499-508.
- HOWE, J. A., SHIMMIELD, T. M., HARLAND, R. and EYLES, N., 2007. Late Quaternary contourites
- and glaciomarine sedimentation in the Fram Strait. Sedimentology, 55 (1): 179-200.
- HÜNEKE, H., 2016. Contourites. In: Harff, J., Meschede, M., Petersen, S. and Thiede, J., Eds.,
- 770 *Encyclopedia of marine geosciences*, doi:10.1007/978-94-007-6238-1 49.
- HÜNEKE, H. and STOW, D. A. V., 2008. Identification of ancient contourites: problems and
- 772 palaeoceanographic significance. In: Rebesco, M. and Camerlenghi, A., Eds., Contourites: developments
- in sedimentology, 60: 323-344. Boston: Elsevier.
- JOHNSON, G. C., STABENO, P. J. and RISER, S. C., 2004. The Bering Slope current system revisited.
- 775 Journal of Physical Oceanography, 34 (2): 384-398.
- JONKERS, L., BARKER, S., HALL, I. R. and PRINS, M. A., 2015. Correcting for the influence of ice-
- rafted detritus on grain size-based paleocurrent speed estimates. *Paleoceanography and*
- 778 *Paleoclimatology*, 30 (10): 1347-1357.
- 779 KANEMATSU, Y., TAKAHASHI, K., KIM, S., ASAHI, H. and KHIM, B. -K., 2013. Changes in
- biogenic opal productivity with Milankovitch cycles during the last 1.3 Ma at IODP Expedition 323 Sites
- 781 U1341, U1343, and U1345 in the Bering Sea. *Quaternary International*, 310: 213-220.
- 782 KASPER ZUBILLAGA, J. and CARRANZA-EDWARDS, A., 2005. Grain size discrimination between
- sands of desert and coastal dunes from northwestern Mexico. Revista Mexicana de Ciencias Geológicas,

- 784 22 (3): 383-390.
- 785 KATSUKI, K. and TAKAHASHI, K., 2005. Diatoms as paleoenvironmental proxies for seasonal
- productivity, sea-ice and surface circulation in the Bering Sea during the late Quaternary. *Deep Sea*
- 787 Research Part II: Topical Studies in Oceanography, 52 (16-18): 2110-2130.
- 788 KAWAGUCHI, Y., NISHIOKA, J., NISHINO, S., YASUDA, I., FUJIWARA, A., LEE, K.,
- 789 YANAGIMOTO, D., MITSUDERA, H. and FUJIO, S., 2020. Cold water upwelling near the Anadyr
- 790 Strait: observations and simulations. *Journal of Geophysical Research: Oceans*, 125:
- 791 https://doi.org/10.1029/2020JC016238.
- 792 KIM, S., YOO, K. -C., LEE, J. I., LEE, M. K., KIM, K., YOON, H. I. and MOON, H. S., 2018.
- Relationship between magnetic susceptibility and sediment grain size since the last glacial period in the
- Southern Ocean off the northern Antarctic Peninsula linkages between the cryosphere and atmospheric
- circulation. *Palaeogeography, Palaeoclimatology, Palaeoecology,* 505: 359-370.
- 796 KINNEY, J. and MASLOWSKI, W., 2012. On the oceanic communication between the Western
- 797 Subarctic Gyre and the deep Bering Sea. Deep Sea Research Part I: Oceanographic Research Papers, 66:
- 798 11-25.
- 799 KRISSEK, L. A., MORLEY, J. J. and LOFLAND, D. K., 1985. The occurrence, abundance, and
- composition of ice-rafted debris in sediments from Deep Sea Drilling Project Sites 579 and 580,
- northwest Pacific. In: Heath, G. R., Burckle, L. H., et al., *Initial Reports of the Deep Sea Drilling Project:*
- 802 86: 647-655. Washington: U.S. Government Printing Office.
- LISIECKI, L. E. and RAYMO, M. E., 2005. A Pliocene-Pleistocene stack of 57 globally distributed
- 804 benthic δ18O records. *Paleoceanography*, 20: doi:10.1029/2004PA001071.
- 805 LISITZIN, A. P., 2002. Sea-ice and iceberg sedimentation in the ocean: recent and past. Berlin:
- Springer, 563 pp.
- 807 LOPEZ, O. M., HEGY, M. C. and MISSIME, T. M., 2020. Statistical comparisons of grain size
- characteristics, hydraulic conductivity, and porosity of barchan desert dunes to coastal dunes. Aeolian
- 809 Research, 43: doi:10.1016/j.aeolia.2020.100576.

- 810 LOUGHLIN, T. R., SUKHANOVA, I. N., SINCLAIR, E. H. and FERRERO, R. C., 1999. Summary of
- biology and coosystem dynamics in the Bering Sea. In: Loughlin, T. R. and Ohtani, K., Eds., *Dynamics of*
- 812 the Bering Sea, Alaska Sea Grant College Program Report, 99-03: 387-407. Fairbanks: University of
- 813 Alaska Sea Grant.
- LOUTRE, M. F. and BERGER, A., 2003. Marine Isotope Stage 11 as an analogue for the present
- 815 interglacial. Global Planetary Change, 36: 209-217.
- 816 LUCCHI, R. G. and REBESCO, M., 2007. Glacial contourities on the Antarctic Peninsula margin: insight
- for palaeoenvironmental and palaeoclimatic conditions. In: Viana A. R. and Rebesco, A. M., Eds.,
- 818 Economic and palaeoceanographic significance of contourite deposits, Geological Society of London
- 819 *Special Publication*, 276: 111-128.
- MAGER, S. M., SMITH, I. J., KEMPEMA, E. W., THOMSON, B. J. and LEONARD, G.H., 2013.
- Anchor ice in polar oceans. *Progress in Physical Geography*, 37 (4): 468-483.
- MAHOWALD, N. M., BAKER, A. R., BERGAMETTI, G., BROOKS, N., DUCE, R. A., JICKELLS, T.
- D., KUBILAY, N., PROSPERO, J. M. and TEGEN, I., 2005. The atmospheric global dust cycle and iron
- 824 inputs to the ocean. Global Biogeochemical Cycles, 19 (4): doi:10.1029/2004GB002402.
- MARTINS, L. R., 2003. Recent sediments and grain-size analysis. *Gravel*, 1: 90-105.
- 826 MARTINS, L. and BARBOZA, E., 2005. Sand-gravel marine deposits and grain-size properties. *Gravel*,
- 827 3: 59-70.
- MASSON, D. G., HARBITZ, C. B., WYNN, R. B., PEDERSON, G. and LØVHOLT, F., 2006.
- 829 Submarine landslides: processes, triggers and hazard prediction. *Philosophical Transactions of the Royal*
- 830 *Society A*, 364: 2009-2039.
- MASSON, D. G., WYNN, R. B. and BETT, B. J., 2004. Sedimentary environment of the Faroe-Shetland
- and Faroe Bank Channels, north-east Atlantic, and the use of bedforms as indicators of bottom current
- velocity in the deep ocean. Sedimentology, 51 (6): 1207-1241.
- 834 MASSON-DELMOTTE, V., DREYFUS, G., BRACONNOT, P., JOHNSEN, S., JOUZEL, J.,
- 835 KAGEYAMA, M., LANDAIS, A., LOUTRE, M. -F., NOUET, J., PARRENIN, F., RAYNAUD, D.,

- 836 STENNI, B. and TUENTER, E., 2006. Past temperature reconstructions from deep ice cores: relevance
- for future climate change. *Climate of the Past*, 2: 399-448.
- MAUCH, M., DURSKI, S. M. and KURAPOV, A. L., 2018. Connectivity of the Aleutian North Slope
- 839 Current and Bering Sea basin waters at the level of the subsurface temperature maximum: a modeling
- 840 study. Journal of Geophysical Research: Oceans, 123 (11): 8608-8623.
- MCCAVE, I. N. and ANDREWS, J. T., 2019. Distinguishing current effects in sediments delivered to the
- ocean by ice. I. Principles, methods and examples. *Quaternary Science Reviews*, 212: 92-107.
- MCCAVE, I. N. and HALL, I. R., 2006. Size sorting in marine muds: processes, pitfalls and prospects for
- paleoflow-speed proxies. Geochemistry, Geophysics, Geosystems, 7 (10): doi:10.1029/2006GC001284.
- MCCAVE, I. N., MANIGHETTI, B. and ROBINSON, S. G., 1995. Sortable silt and fine sediment
- size/composition slicing: parameters for palaeocurrent speed and palaeoceanography. *Paleoceanography*,
- 847 10: 593-610.
- MCCAVE, I. N., THORNALLEY, D. J. R. and HALL, I. R., 2017. Relation of sortable silt grain-size to
- deep-sea current speeds: calibration of the 'mud current meter'. Deep Sea Research Part I:
- 850 Oceanographic Research Papers, 127: 1-12.
- MCLAREN, P., 1981. An interpretation of trends in grain size measures. *Journal of Sedimentary*
- 852 *Research*, 51 (2): 611-624.
- MCMANUS, J., 1988. Grain size determination and interpretation. In: Tucker, M., Ed., *Techniques in*
- 854 *sedimentology*, 63-85. Boston: Blackwell Scientific Publications.
- MÉHEUST, M., STEIN, R., FAHL, K. and GERSONDE, R., 2018. Sea-ice variability in the subarctic
- North Pacific and adjacent Bering Sea during the past 25 ka: new insights from IP25 and Uk'37 proxy
- 857 records. Arktos, 4 (8): doi:10.1007/s41063-018-0043-1.
- MICHELS, K. H., ROGENHAGEN, J. and KUHN, G., 2001. Recognition of contour-current influence in
- mixed contourite-turbidite sequences of the western Weddell Sea, Antarctica. Marine Geophysical
- 860 Research, 22: 465-485.

- 861 MUHONG, C., FAN, Z., JUN, L., SHANGBIN, X., WEN, Y., ZHONG, C., RONG, X., GANGJIAN, W.
- and LANLAN, Z., 2005. Original component of grain size index in core sediment from southwestern
- slope of the South China Sea and its paleoenvironmental implication. Chinese Science Bulletin, 50: 896-
- 864 902.
- 865 MULDER, T., HASSAN, R., DUCASSOU, E., ZARAGOSI, S., GONTHIER, E., HANQUIEZ, V.,
- MARCHÈS, E. and TOUCANNE, S., 2013. Contourites in the Gulf of Cadiz: a cautionary note on
- potentially ambiguous indicators of bottom current velocity. *Geo-Marine Letters*, 33: 357-367.
- NAGASHIMA, K., ASAHARA, Y., TAKEUCHI, F., HARADA, N. and TADA, R., 2012. Contribution
- of detrital materials from the Yukon River to the continental shelf sediments of the Bering Sea based on
- 870 the ESR intensity and crystallinity of quartz. Deep Sea Research Part II: Topical Studies in
- 871 *Oceanography*, 61-64: 145-154.
- NAIDU, A. S. and MOWATT, T. C., 1983. Sources and dispersal patterns of clay minerals in surface
- sediments from the continental shelf areas off Alaska. *Geological Society of America Bulletin*, 94 (7):
- 874 841-854.
- 875 NELSON, C. H., 1982. Late Pleistocene Holocene transgressive sedimentation in deltaic and non-deltaic
- areas of the northeastern Bering epicontinental shelf. Geologie En Mijnbouw 61:5-18.
- 877 NESTEROVICH, A., 2019. Quantitative diatom-based proxy for sea ice extent in the Bering and Chukchi
- seas. Ph.D thesis, Iowa State University, https://dr.lib.iastate.edu/handle/20.500.12876/31460.
- NOAA NATIONAL GEOPHYSICAL DATA CENTER., 2009. ETOPO1 1 Arc-Minute Global Relief
- Model. NOAA National Centers for Environmental Information. Accessed [March 16, 2016].
- NÜRNBERG, D., WOLLENBERG, I., DETHLEFF, D., EICKEN, H., KASSENS, H., LETZIG, T.,
- REIMNITZ, E. and THIEDE, J., 1994. Sediments in Arctic sea ice: implications for entrainment,
- transport and release. Marine Geology, 119 (3-4): 185-214.
- 884 ONODERA, J., TAKAHASHI, K. and NAGATOMO, R., 2016. Diatoms, silicoflagellates, and ebridians
- at Site U1341 on the western slope of Bowers Ridge, IODP Expedition 323. Deep Sea Research Part II:
- 886 Topical Studies in Oceanography, 125-126: 8-17.

- O'REGAN, M., SELLÉN, E. and JAKOBSSON, M., 2014. Middle to late Quaternary grain size
- variations and sea-ice rafting on the Lomonosov Ridge. *Polar Research*, 33 (1):
- 889 doi:10.3402/polar.v33.23672.
- 890 PALUMBO, E., VOELKER, A. H. L., FLORES, J. A. and AMORE, O. F., 2019. Surface-ocean
- dynamics during eccentricity minima: a comparison between interglacial Marine Isotope Stage (MIS) 1
- and MIS 11 on the Iberian Margin. *Global Planetary Change*, 172: 242-255.
- PELTO, B. M., CAISSIE, B. E., PETSCH, S. T. and BRIGHAM-GRETTE, J., 2018. Oceanographic and
- 894 climatic change in the Bering Sea, Last Glacial Maximum to Holocene. Paleoceanography and
- 895 *Paleoclimatology*, 33 (1): 93-111.
- 896 POPPE, L. J., WILLIAMS, S. J. and PASKEVICH, V. F., 2006. Textural analysis of marine sediments at
- the USGS Woods Hole Science Center; methodology and data on DVD. Proceedings of the Joint Eighth
- 898 Federal Interagency Sedimentation Conference, Reno, 2006: 905-911.
- 899 PRANTS, S. V., ANDREEV, A. G., YU ULEYSKY, M. and BUDYANSKY, M. V., 2019. Lagrangian
- study of mesoscale circulation in the Alaskan Stream area and the eastern Bering Sea. Deep Sea Research
- 901 *Part II: Topical Studies in Oceanography*, 169-170: https://doi.org/10.1016/j.dsr2.2019.03.005.
- 902 REBESCO, M., HERNÁNDEZ-MOLINA, F. J., VAN ROOIJ, D. and WAHLIN, A., 2014. Contourites
- and associated sediments controlled by deep-water circulation processes: State-of-the-art and future
- 904 considerations. Marine Geology, 352: 111-154.
- 905 REIMNITZ, E., MCCORMICK, M., BISCHOF J. and DARBY, D., 1998. Comparing sea-ice sediment
- load with Beaufort Sea shelf deposits: is entrainment selective? *Journal of Sedimentary Research*, 68 (5):
- 907 777-787.
- 908 RICHWINE, K. A., SMITH, K. R. and MCCONNAUGHEY, R. A., 2018. Surficial sediments of the
- 909 eastern Bering Sea continental shelf: EBSSED-2 database documentation. U.S. Department of Commerce,
- 910 NOAA Technical Memorandum NMFS-AFSC, 377: 48 pp.

- 911 RIETHDORF, J. R., NÜRNBERG, D., MAX, L., TIEDEMANN, R., GORBARENKO, S. A. and
- 912 MALAKHOV, M. I., 2013. Millennial-scale variability of marine productivity and terrigenous matter
- 913 supply in the western Bering Sea over the past 180 kyr. Climate of the Past, 9: 1345-1373.
- Positive Rothwell, R. G. and RACK., F. R., 2006. New techniques in sediment core analysis: an introduction.
- 915 In: Rothwell, R. G., Ed., New techniques in sediment core analysis, Geological Society of London Special
- 916 *Publications*, 267: 1-29.
- 917 RUDDIMAN, W. F., 1977. Late Quaternary deposition of ice-rafted sand in the subpolar North Atlantic
- 918 (lat 40° to 65°N). Geological Society of America Bulletin, 88: 1813-1827.
- 919 RUDDIMAN, W. F., 2007. The early anthropogenic hypothesis: challenges and responses. Review of
- 920 *Geophysics*, 45: https://doi.org/10.1029/2006RG000207.
- 921 SAKAMOTO, T., IKEHARA, M., AOKI, K., IIJIMA, K., KIMURA, N., NAKATSUKA, T. and
- WAKATSUCHI, M., 2005. Ice-rafted debris (IRD)-based sea-ice expansion events during the past 100
- 923 kyrs in the Okhotsk Sea. Deep Sea Research Part II: Topical Studies in Oceanography, 52 (16-18): 2275-
- 924 2301.
- 925 SANCETTA, C., HEUSSER, L., LABEYRIE, L., NAIDU, A. S. and ROBINSON, S. W., 1985.
- 926 Wisconsin—Holocene paleoenvironment of the Bering Sea: evidence from diatoms, pollen, oxygen
- 927 isotopes and clay minerals. *Marine Geology*, 62 (1-2): 55-68.
- 928 SHAFFER, G. and LAMBERT, F., 2018. In and out of glacial extremes by way of dust-climate
- 929 feedbacks. Proceedings of the National Academy of Sciences, 115 (9): 2026-2031.
- 930 SCHLEE, J., 1973. Atlantic continental shelf and slope of the United States: sediment texture of the
- Northeastern part. U.S. Geological Survey Professional Paper, 529-L: 63 pp.
- 932 SEQUEIROS, O. E., MOSQUERA, R. and PEDOCCHI, F., 2018. Internal structure of a self-accelerating
- turbidity current. *Journal of Geophysical Research: Oceans*, 123: 6260-6276.
- 934 SERNO, S., WINCKLER, G., ANDERSON, R., HAYES, C., MCGEE, D., MACHALETT, B., REN, H.,
- 935 STRAUB, S. M., GERSONDE, R. and HAUG, G. H., 2014. Eolian dust input to the Subarctic North
- 936 Pacific. Earth and Planetary Science Letters, 387, 252-263.

- 937 SEVON, W. D., 1966. Distinction of New Zealand beach, dune, and river sands by their grain size
- 938 distribution characteristics. New Zealand Journal of Geology and Geophysics, 9 (3): 212-223.
- 939 SHARMA, G. D., 1975. Contemporary epicontinental sedimentation and shelf grading in the southeast
- 940 Bering Sea. In: Forbes, R. B., Ed., Contributions to the geology of the Bering Sea Basin and adjacent
- 941 regions, Geological Society of America Special Paper, 151: 33-48.
- 942 SIGLER, M. F., HARVEY, H. R., ASHJIAN, J., LOMAS, M. W., NAPP, J. M., STABENO, P. J. and
- VAN PELT, T. I., 2010. How does climate change affect the Bering Sea ecosystem? EOS, 91 (48): 457-
- 944 458.
- 945 SPRINGER, A., MCROY, C. and FLINT, M., 1996. The Bering Sea Green Belt: shelf-edge processes
- and ecosystem production. Fisheries Oceanography, 5 (3-4): 205-223.
- 947 ST. JOHN, K., 2008. Cenozoic ice-rafting history of the central Arctic Ocean: terrigenous sands on the
- 948 Lomonosov Ridge. *Paleoceanography*, 23: doi:10.1029/2007PA001483.
- 949 ST. JOHN, K., PASSCHIER, S., TANTILLO, B., DARBY, D. and KEARNS, L., 2015. Microfeatures of
- 950 modern sea-ice-rafted sediment and implications for paleo-sea-ice reconstructions. Annals of Glaciology,
- 951 56 (69): 83-93.
- 952 STABENO, P. J., DANIELSON, S., KACHEL, D., KACHEL, N.B. and MORDY, C.W., 2016. Currents
- and transport on the eastern Bering Sea shelf: An integration of over 20 years of data. *Deep Sea Research*
- 954 Part II: Topical Studies in Oceanography, 134: 13–29.
- 955 STABENO, P. J., KACHEL, D. G., KACHEL, N. B. and SULLIVAN, M. E., 2005. Observations from
- moorings in the Aleutian Passes: temperature, salinity and transport. Fisheries Oceanography, 14: 39-54.
- 957 STABENO, P. J., LADD, C. and REED, R.K., 2009. Observations of the Aleutian North Slope Current,
- 958 Bering Sea, 1996–2001. Journal of Geophysical Research: Oceans, 114.
- 959 https://doi.org/10.1029/2007JC004705.
- 960 STABENO, P. J., SCHUMACHER, J. D. and OHTANI, K., 1999. The physical oceanography of the
- 961 Bering Sea. In: Loughlin, T. R. and Ohtani, K., Eds., Dynamics of the Bering Sea, Alaska Sea Grant
- 962 College Program Report, 99-03: 1-28. Fairbanks: University of Alaska Sea Grant.

- 963 STABENO, P. J., THOMAN, R. L. and WOOD, K., 2019. Recent warming in the Bering Sea and its
- impact on the ecosystem. In: Richter-Menge, J., Druckenmiller, M. L. and Jeffries, M., Eds., Arctic
- 965 Report Card 2019, https://arctic.noaa.gov/Report-Card/Report-Card-2019.
- 966 STOW, D. A. V. and FAUGÈRES, J. -C., 2008. Contourite facies and the facies model. In: Rebesco, M.
- and Camerlenghi, A., Eds., Contourites: developments in sedimentology, 60: 223-256. Boston: Elsevier.
- 968 STOW, D. A. V., FAUGÈRES, J. -C., HOWE, J. A., PUDSEY, C. J. and VIANA, A. R., 2002. Bottom
- currents, contourities and deep-sea sediment drifts: current state-of-the-art. In: Stow, D. A. V., Pudsey, C.
- 970 J., Howe, J. A., Faugères, J. -C and Viana, A. R., Eds., Deep-water contourite systems: modern drifts and
- ancient series, seismic and sedimentary characteristics, Geologic Society of London Memoirs, 22: 7-20.
- 972 STOW, D. and SMILLIE, Z., 2020. Distinguishing between deep-water sediment facies: turbidites,
- 973 contourites and hemipelagites. *Geosciences*, 10 (2): doi:10.3390/geosciences10020068.
- 974 STOW, D. A. V. and TABREZ, A. R., 1998. Hemipelagites: processes, facies and model. In: Stoker, M.
- 975 S., Evans, D. and Cramp, A., Eds., Geological processes on continental margins: sedimentation, mass
- 976 wasting and stability, Geological Society of London Special Publication, 129: 317-337.
- 977 STUUT, J. -B. W., TEMMESFELD, F. and DE DECKKER, P., 2014. A 550 ka record of aeolian activity
- 978 near North West Cape, Australia: inferences from grain-size distributions and bulk chemistry of SE
- 979 Indian Ocean deep-sea sediments. *Quaternary Science Reviews*, 83: 83-94.
- 980 SVAL'NOV, V. N. and ALEKSEEVA, T. N., 2006. Characteristics of the grain-size composition of
- deep-water oceanic sediments. Lithology and Mineral Resources, 41 (3): 201-214.
- TAKAHASHI, K., RAVELO, A. C., ALVAREZ ZARIKIAN, C. A., and EXPEDITION 323
- 983 SCIENTISTS, 2011. Proceedings of the Integrated Ocean Drilling Program, 323. doi:10.2204/
- 984 iodp.proc.323.2011.
- TEGEZ, A. D., JANSEN, E., and TELFORD, R. J., 2014. The role of the northward-directed (sub)surface
- limb of the Atlantic Meridional Overturning Circulation during the 8.2 ka event. Climate of the Past, 10:
- 987 1887-1904. doi:10.5194/cp-10-1887-2014.

- 988 THOMPSON, N. AND CAISSIE, B. (2021). Grain size records from Bering Sea core sites U1345,
- 989 U1343, and U1339 during Marine Isotope Stage 11 (424-374 thousand years ago). Arctic Data
- 990 Center. https://doi.org/10.18739/A2H12V839.
- 991 TOUCANNE, S., MULDER, T., SCHÖNFELD, J., HANQUIEZ, V., GONTHIER, E., DUPRAT, J.,
- 992 CREMER, M., ZARAGOSI, S., 2007. Contourites of the Gulf of Cadiz: a high-resolution record of the
- 993 paleocirculation of the Mediterranean outflow water during the last 50,000 years. *Palaeogeography*
- 994 *Palaeoclimatology, Palaeoecology,* 246: 354-366. doi:10.1016/j.palaeo.2006.10.007.
- 995 UDDEN, J. A., 1914. Mechanical composition of clastic sediments. *Geological Society of America*
- 996 Bulletin, 25(1): 655-744. doi:10.1130/GSAB-25-655.
- 997 VAUGHN, D. R. and CAISSIE, B. E., 2017. Effects of sea-level, sea-ice extent, and nutrient availability
- on primary production at the Umnak Plateau, Bering Sea (IODP Site U1339) during Marine Isotope Stage
- 999 (MIS) 5. Palaeogeography Palaeoclimatology, Palaeoecology, 485: 283-292.
- 1000 doi:10.1016/j.palaeo.2017.06.020.
- 1001 VOELKER, A. H. L., LEBREIRO, S. M., SCHONFELD, J., CACHO, I., ERLENKEUSER, H., and
- ABRANTES, F., 2006. Mediterranean outflow strengthening during northern hemisphere coolings: a salt
- source for the glacial Atlantic? Earth and Planetary Science Letters, 245(1-2): 39-55.
- 1004 doi:10.1016/j.epsl.2006.03.014.
- 1005 VOIGT, I., CHIESSI, C.M., PIOLA, A.R., and HEINRICH, R., 2016. Holocene changes in Antarctic
- 1006 Intermediate Water flow strength in the Southwest Atlantic. Palaeogeography Palaeoclimatology,
- 1007 *Palaeoecology*, 463: 60-67. doi:10.1016/j.palaeo.2016.09.018.
- 1008 VON HUENE, R., LARSON, E., AND CROUCH, J., 1973. Preliminary study of ice rafted erratics as
- indicators of glacial advances in the Gulf of Alaska. Deep Sea Drilling Project Initial Reports, 18: 835-
- 1010 842.
- 1011 WANG, R., BISKABORN, B.K., RAMISCH, A., REN, J., ZHANG, Y., GERSONDE, R., and
- DIEKMANN, B., 2016. Modern modes of provenance and dispersal of terrigenous sediments in the North

- Pacific and Bering Sea: implications and perspectives for palaeoenvironmental reconstructions. Geo-
- 1014 *Marine Letters*, 36(4): 259-270. doi:10.1007/s00367-016-0445-7.
- WARNER, N. and DOMACK, E., 2002. Millennial- to decadal scale paleoenvironmental change during
- the Holocene in the Palmer Deep, Antarctica, as recorded by particle size analysis. *Paleoceanography*,
- 1017 17(3): 8004. doi:10.1029/2000PA000602.
- WARRIER, A.K., PEDNEKAR, H., MAHESH, B.S., MOHAN, R., and GAZI, S., 2016. Sediment grain
- size and surface textural observations of quartz grains in late quaternary lacustrine sediments from
- Schirmacher Oasis, East Antarctica: Paleoenvironmental significance. *Polar Science*, 10(1): 89-100.
- 1021 doi:10.1016/j.polar.2015.12.005.
- WELTJE, G. and PRINS, M., 2003. Muddled or mixed? Inferring paleoclimate from size distributions of
- deep-sea clastics. Sedimentary Geology, 162: 39-62. doi:10.1016/S0037-0738(03)00235-5.
- WENTWORTH, C.K., 1922. A scale of grade and class terms for clastic sediments. *The Journal of*
- 1025 *Geology*, 30(5): 377-392.
- WOLF-WELLING, T., CREMER, M., OCONNELL, S., WINKLER, A., and THIEDE, J., 1996.
- 1027 Cenozoic Arctic gateway paleoclimate variability: indications from changes in coarse-fraction
- 1028 composition. *Proceedings of the Ocean Drilling Program, Scientific Results*, 151: 515-567.
- 1029 doi:10.2973/odp.proc.sr.151.139.1996.
- 1030 WU, L., WANG, R., XIAO, W., KRIJGSMAN, W., LI, Q., GE, S., and MA, T., 2018. Late Quaternary
- deep stratification-climate coupling in the Southern Ocean: implications for changes in abyssal carbon
- 1032 storage. Geochemistry, Geophysics, Geosystems, 19(2): 379-395. doi:10.1002/2017GC007250.
- 1033 ZIMMERMANN, M. and PRESCOTT, M. M., 2018. Bathymetry and canyons of the Eastern Bering Sea
- 1034 Slope. *Geosciences*, 8(5): 184.